5-2023

DPD Guided Insight on the Formation Process of Polyethersulfone Membranes by Nonsolvent Induced Phase Separation and the Effects of Additives

Eric Ledieu
University of Arkansas, Fayetteville

DPD Guided Insight on the Formation Process of Polyethersulfone Membranes by Nonsolvent Induced Phase Separation and the Effects of Additives

A thesis submitted in partial fulfillment
of the requirements for a degree of
Master of Science in Biomedical Engineering

by

Eric Ledieu
University of the Ozarks
Bachelor of Science in Biology and Chemistry, 2018

May 2023
University of Arkansas

This thesis is approved for recommendation to the Graduate Council.

Xianghong Qian, Ph.D.
Thesis Director

Ranil Wickramasinghe, Ph. D
Committee member

Paul Millett, Ph. D.
Committee member

Jeffery Wolchok, Ph. D.
Committee Member

Abstract

Dissipative particle dynamics (DPD), a coarse grain simulation method, was applied to the membrane formation process of non-solvent induced phase separation (NIPS) to gain further insight on the mechanism of certain variables and how they affect the final morphology. NIPS involves two solutions, an organic polymer dissolved in an organic solvent colloquially called the dope and an aqueous coagulation bath, brought into contact with one another. The solvents then mix, causing the polymer to fall out of solution as an asymmetric membrane with a dense surface layer and a more open subsurface layer in response to the decreasing solubility. Polyethersulfone (PES), a common industrial choice we have previously studied, was utilized as the polymer with N-methyl-2-pyrrolidone (NMP) as the organic solvent and water as the coagulation bath. In this study, our previous model construction was altered in several ways. Firstly, the simulation area was enlarged, allowing for a better sampling of subsurface behavior. Secondly, polymer chain length was increased to bring it more in line with the high molecular weight of industrially common polymers, with our experimental systems ranging from 100 to 200 monomers. Lastly, polyvinylpyrrolidone (PVP) was introduced as an additive to the polymer solution in concentrations varying from 1 to 10% by volume of the dope. PVP is a common polymer additive utilized in industry to produce larger pores, a result that was successfully replicated. We also investigated the effects of adding solvent to the coagulation bath as well as the effects of adding water to the polymer solution.

Table of Contents

DPD Guided Insight on the Formation Process of Polyethersulfone Membranes by Nonsolvent Induced Phase Separation and the Effects of Additives

Introduction....1
Chapter 1: Membrane Fundamentals and Common Concerns....1
1.1 Types and Basic Characteristics....1
1.2 Fouling and Mitigation....3
1.3 Alternative Application of Membranes....5
Chapter 2: Membrane Formation and Manufacturing....7
2.1 Manufacturing Processes....7
2.2 Controlling Structure....10
2.3 Additives....14
2.4 Figures....16
Figure 2.1....16
Figure 2.2....17
Chapter 3: Computational Approaches....18
3.1 Overview of Simulation Methods....18
3.2 DPD Modeling....19
3.3 Tables....24
Table 3.1....24
Table 3.2....24
Chapter 4: Simulation Investigation of Membrane Making....25
4.1 System Construction....25
4.2 Experimental Sets....26
Molecular Weight....26
Coagulant in the Polymer Solution....27
Solvent in Coagulation Bath....27
PVP additive....27
4.3 Results and Discussion....28
Molecular Weight....28
Water in the Polymer Solution....30
Solvent in Coagulation Bath....31
PVP Additive....32

4.4 Conclusion....33
4.5 Tables and Figures....36
Table 4.1....36
Table 4.2....36
Table 4.3....36
Table 4.4....37
Table 4.5a....37
Table 4.5b....38
Figure 4.1....38
Experimental Set 1....39
Figure 4.2....39
Experimental Set 2....40
Figure 4.3....41
Experimental Set 3....42
Figure 4.4....42
Experimental Set 4....43
Figure 4.5....43
Figure 4.6....44
Figure 4.7....45
Literature Cited....47

List of Abbreviations and Variables

γ	: Activity Coefficient in eq 10; also a dissipative coefficient in eq 12
φ	: Volume fraction
δ_D	: Dispersion component of the Hansen solubility parameter
δ_H	: Hydrogen bonding component of the Hansen solubility parameter
δ_P	: Polarity component of the Hansen solubility parameter
$\widetilde{\vec{v}_i}(t)$	: Estimated velocity of particle i at time t
$\overrightarrow{F_{ij}^C}$	: Conservative force applied by interaction with particle j on particle i
$\overrightarrow{e_{ij}}$	: directional unit vector from particle i and j
$\vec{f}_i(t)$	: Force acting on particle i at time t
$\vec{r}_i(t)$	: Position of particle i at time t
$\vec{v}_i$	: Velocity of particle i at time t
T_{ref}	: Reference temperature (273 K)
a_{ij}	: interaction parameter between particle i and j
k_b	: Boltzmann constant
r_c	: Cutoff radius (0.84 nm)
r_{ij}	: distance between particle i and j
θ_{ij}	: Random number generated for the random force
χ_{ij}	: Flory-Huggins interaction parameter for particle i and j
ω^D	: Weighting coefficient for the dissipative force
ω^R	: Weighting coefficient for the random force
Δt	: Time step
A	: PVP additive
C	: Water bead
CA	: Cellulose acetate
CHARMM	: Chemistry at Harvard Macromolecular Mechanics
-COOH	: Carboxyl group
DMAc	: Dimethylacetamide
DMF	: Dimethylformamide
DMSO	: Dimethyl sulfoxide
DPD	: Dissipative particle dynamics
HMPA	: Hexamethylphosphoramide
MD	: Molecular dynamics
NF	: Nanofiltration
NIPS	: Nonsolvent induced phase separation
NMP	: n-methyl-2-pyrrolidone
-OH	: Hydroxyl group
P	: PES bead
PAN	: Polyacrylonitrile
PEG	: Polyethylene glycol
PEI	: Polyether Amide
PES	: Polyethersulfone
PI	: Polyimide
PS	: Polysulfone
PVDF	: Polyvinylidene fluoride
PVP	: Polyvinylpyrrolidone
RO	: Reverse osmosis
S	: NMP solvent bead

TIPS	: Temperature induced phase separation
UF	: Ultrafiltration
VIPS	: Vapor induced phase separation
σ	: Temperature based coefficient for the random force (set to 3)
M	: Mass
τ	: Reduced time unit (7.9 ps)

Introduction

Polymeric membranes have seen an increasingly wide usage in a variety of applications, with an ever-growing number of papers investigating their most common manufacturing process, phase inversion, alone, going from 34 in the 1980s, 341 in the 1990s, and a staggering 1263 in the 2000s (Guillen, et al. 2011). These membranes have wide applications depending on their morphologies, ranging from non-porous membranes serving for gas separation application, reverse osmosis (RO) membranes utilized in desalination, ultrafiltration and nanofiltration membranes seeing usage in protein purification, and microfiltration serving for both bulk material removal and as support layers and structures for other membrane types, such as osmotic distillation membranes (Shen, Han and Wickramasinghe 2004) (Drioli, Giorno and Macedonio 2019).

Chapter 1: Membrane Fundamentals and Common Concerns

1.1 Types and Basic Characteristics

While there are other types of membranes, one of the most popular functions is a size exclusion mechanism. This mechanism is a pressure driven filtration system in which the feed is passed through the membrane in one of two modes, using the size of the pores for separation. The first of these two modes are dead end, which involves the feed being pressurized directly onto the membrane surface, causing the deposition of a cake layer composed of particulate that could not pass through. The other is tangential flow, in which the membrane surrounds the feed, but the feed has an escape to some other downstream process, becoming what is known as the retentate. This retentate can undergo dilution and recirculation through the purification process, disposal, or any other fate specific to the industrial application.

Depending on the scale of the particulate being rejected, these membranes are divided into broad categories. The exact boundary of these definitions are blurry, but are presented here as the best

working consensus available. At the broadest, microfiltration (sometimes abbreviated to MF) membranes tend to have pores in the 0.1 µm to 10 µm range, which can typically block suspended solids, bacteria, and large fat globules. The next category is ultrafiltration (sometimes abbreviated to UF), which allows small molecules, such as sugars, salts, small acids, and small peptides through with pore sizes in the 100 nm to 10 nm. These are useful in protein purification and other such small-scale separations, but do not work for desalination or other molecular separations. The last porous membrane category is nanofiltration, which ranges from 1 nm to 10 nm and is utilized to remove small molecules, such as simple sugars, any organic matter, or larger ions. Lastly, reverse osmosis involves a thin nonporous layer through which water permeates, but rejects monovalent ions.

To effectively characterize these membranes, a series of physical properties need to be considered. First, there are the simple functioning mechanical properties. These are the largest pore size, which is the limit in selectivity, the pore size distribution, as a wide distribution results in poor flow as smaller pores do not have as much flux as large ones, and pore length, as longer pores have lower flux. On that last point, the tortuosity of the pore matters as a thin membrane with tortuous pores is equivalent to a thicker membrane with straighter pores. A higher porosity, or open volume in the membrane, is also desirable for its benefit to flow rate. There are other considerations for usage, of course. For example, the material needs to be resistant to the chemical environment for use and mechanically resistant to pressure and temperature conditions, which limit our material choices. Similarly, fouling is a major usage concern which has been a continuing area of research. Fouling is the accumulation of contaminants onto the membrane surface, thereby clogging pores, causing membrane deformation, or changing the surface properties of the membrane and can behave differently based on a variety of factors (Guo, Ngo and Li 2012). As the flow rate is decreased by foulants, the transmembrane pressure must be increased to compensate, causing higher energy consumption. Furthermore, the concentration

polarization at the surface of the membrane is increased by fouling, causing a lower rate of rejection and decreasing performance. Furthermore, fouling can occur at any point of the membrane, including the inside of pores, which is difficult to clean. Fouling on the inside of the membrane is of course more common for membranes with larger pores, such as microfiltration or ultrafiltration, while foulants tend to remain at the surface for reverse osmosis (Zhao, et al. 2021).

1.2 Fouling and Mitigation

Foulants are divided into four major categories. First, particulates are particles that physically bind to the membrane, reducing transport by occluding pores. These are largely in the 1 nm to 1 µm as smaller particles tend to diffuse away from the membrane by molecular diffusion while larger ones are removed using shear flow. While this class of foulants has particles that fit in other categories, these are pulled apart as their fouling mechanism is simple deposition rather that more specific interactions with the membrane or other foulants (Zhao, et al. 2021). The second broad category is organics and is composed of colloids and dissolved components that attach by adsorption to the membrane. For common cases such as water treatment, this organic matter is largely composed of small hydrophobic acids, proteins, and amino acids as well as larger molecules, such as humic and fulvic acids. The initial stages of this type of fouling appear to be largely driven by 300-1000 Da molecules, while larger molecules dominated later fouling layer growth (Zhao, et al. 2021) (Lee, Chen and Fane 2008). The third category is Inorganics. These form scales on the membrane when they precipitate due to such factors as pH change, oxidation, or coagulants. Most commonly, however, they form when they become super saturated. Of course, this means salt with low solubility such as calcium sulfate, calcium carbonate, silica, and barium sulfate are commonly found to form scales as they are both common and have lower critical concentration (Zhao, et al. 2021). Lastly, biofilm is formed as microbiological organisms that cling to and replicate on the membrane, forming a gel like layer that is composed of cells as well as extracellular polymeric substances, such as polysaccharides, proteins, lips, nucleic acids,

and combinations therein (Guo, Ngo and Li 2012). This is a particularly pernicious problem plaguing sensitive membranes such as reverse osmosis, as bacteria grow and reproduce. They cannot be easily removed as they can repopulate and are nearly unavoidable, as bacteria come in with the feed unless your feed has been perfectly cleaned. Furthermore, they are generally difficult to detach and clean even when dead. The only two methods that have seen any major success at mitigating this issue are limiting the nutrients in the feed and disinfecting the feed. Disinfecting can come with its own issues as some materials, such as TFC polyamide, can break down due to chloride degradation (Zhao, et al. 2021).

A variety of techniques have been developed to mitigate the damage caused by foulants. Some use chemical washing such as sodium hypochlorite (Rana and Matsuura 2010) while others use mechanical cleaning techniques such as ultrasound (Ahmad, et al. 2012), backflushing (Wang, et al. 2014), and pneumatic cleaning, also known as air scouring (Lin, Lee and Huang 2010). While some fouling can be reversed through cleaning, much is not, and each cycle of cleaning marks a permanent decrease in membrane performance, leading to focus on fouling prevention.

The operating conditions, such as flux and temperature, and the feed characteristics, such as pH and concentration, play a large role in fouling but altering those may be a unique challenge with secondary effect. for example, altering the pH during a protein purification will alter the charge and conformation of the protein. While some of these can be undertaken, a more fouling resistant membrane can work within the limitation and in conjunction with any improvement from the system conditions. Designing the membranes to be less susceptible to fouling in the first place is therefore an ongoing area of research. On a mechanical level, microstructure can be used to promote turbulence, preventing deposition (Jiang, et al. 2021) (Jiang, et al. 2020). On the chemical level, organic and inorganic foulants attach to the membrane through interaction with the membrane surface, such as electrostatic, hydrophobic, van der Waal, or hydrogen bonding. The growing foulant aggregate then grows through the highly favorable foulant-foulant interaction

(Zhao, et al. 2021). As such, it is an effective though difficult strategy to minimize foulant-membrane interactions, thereby preventing the process from starting. Surface chemical composition plays a large role in determining fouling susceptibility, as properties such as charge and hydrophobicity flow from it. As such, introducing functional groups has led to much success, especially oxygen containing groups such as -COOH (Vatanpour, et al. 2011) (Li, et al. 2020), -OH (Zhu, et al. 2017), and -SO_3H (Ayyaru and Ahn 2017) or biocidal agents to reduce biofouling potential. Hydrophilic polyvinyl alcohol coatings are often used in industry for decreasing surface roughness and increasing surface hydrophilicity. Hydrophilicity is often one of the most important predictors of fouling, especially for RO applications (Zhao, et al. 2021). This can be achieved through surface modification, as described above, or through other techniques such as incorporating hydrophilic nanoparticles (Wang, et al. 2019) or introducing a zwitterionic component (Tirado, et al. 2016). Surface modification has a major drawback, however. It may lack stability and may get removed through usage or repeated cleaning cycles.

1.3 Alternative Application Membranes

Despite challenges with fouling, membranes have seen increasingly widespread use across a variety of classes of membranes with unique uses. While the most classic case is a size exclusion membrane, which uses pore size as the main separation principle, there are other principles which also utilize polymer membranes. Some of these, in a bit more detail, include membrane distillation techniques, which are an upcoming technology using polymer membranes to create an air gap that can only be crossed by water vapor (Alkhudhiri, Darwish and Hilal 2012). The process is driven by the differential vapor pressure from the surface of the two membranes, causing condensation on the distillate side to be faster than the one on the feed. The air gap is maintained by using a hydrophobic microfiltration membrane that cannot be wetted, a type of membrane with larger pores than its main competitor, reverse osmosis, which lowers fouling susceptibility.

Another class of membrane are ion exchange membranes. These have embedded charges in the polymer matrix through the grafting of charged groups to the polymer fiber. Notable charged groups include but are not limited to $-SO^{3-}$, $-COO^{-}$, $-PO^{2-}$, $-AsO_3^{2-}$, and $-SeO_3^{-}$ for anionic groups and $-NR_3^{+}$, $-NHR_2^{+}$, $-NH_2R^{+}$, $-PR_3^{+}$, and $-PS_2^{+}$ for cationic groups. The charges then repel similarly charged elements in the feed (co-ions) while allowing the passage of oppositely charged ions (counter-ions). These have a variety of uses as key components of electrodialysis, diffusion dialysis, electrolysis, and flow batteries. New applications are emerging as well in processes such as membrane capacitive deionization, reverse electrodialysis, microbial fuel cells, and ion exchange membrane bioreactors (Luo, Abdu and Wessling 2018). These are but a couple of possible applications for polymeric membrane, but more exist and refinement continues to be an area of interest.

Chapter 2: Membrane Formation and Manufacturing

2.1 Manufacturing Processes

There are several techniques for making polymer membranes. While the focus of this thesis, nonsolvent induced phase separation (NIPS), is a very common industrialized method, there are others. Among those, others also rely on phase separation, notably vapor induced phase separation (VIPS), temperature induced phase separation (TIPS), and solvent evaporation. Phase separation is one of the most common types of membranes used in industry due to the ease of mass manufacture compared to other methods (J. F. Kim, et al. 2012). While the name is self-explanatory as to the mechanism used to produce these membranes, they have their pros and cons. VIPS involves the contact of non-solvent vapors coming into contact with a solvent/polymer mix, causing the decreasingly soluble polymer to fall out of solution. This process is similar to NIPS, which will be discussed more thoroughly below, but the slower mass transfer results in a more controlled process. Once the initial phase separation has occurred, the membrane is either finished or washed using a nonsolvent bath, which is similar to the NIPS (Venault, et al. 2013). This does represent a multistep batch process, which is a slower manufacturing process. TIPS, as the name implies, is induced due to a temperature shift. Less versatile and VIPS or NIPS, TIPS has seen increased interest due to its simplicity, resistance to defects, and reproducibility. It also offers some attractive properties such as high porosity and narrow pore distribution, making the results highly reliable and high flux. The process follows four basic steps. First, a polymer is mixed with a high boiling point solvent with low molecular weight and heated past the melting point of the polymer. Next, the solution is cast into the desired shape. The solution is then allowed to cool, allowing the polymer to fall out of solution as it cools below its melting point. Lastly, the diluent is removed, usually through solvent extraction. This process is very simple and only has two components, as opposed to the three found in other common phase inversion methods, but requires much more energy than NIPS or VIPS, as the melting

temperature of the polymer has to be much hotter than the operating temperature to prevent thermal damage during operation (J. F. Kim, et al. 2012). Still, it remains the second most popular manufacturing method, behind NIPS.

Nonsolvent induced phase separation (NIPS) is a common manufacturing process utilized to fabricate polymer membranes, and the focus of this thesis. The basic procedure for this process consists of a few steps. Assuming that the feed is aqueous, a thin layer of a solution consisting of an organic polymer dissolved in a water miscible organic solvent is cast into shape. This is done in a variety of ways for different shapes. For a lab scale flat sheet membrane, the solution is poured on a glass plate, then the excess is scraped away using a casting knife, leaving a layer of uniform height. The casting knife is a metal bar with a slightly thinner center, so that when the bar is passed over the solution, the polymer solution is scraped to the height of the offset, allowing for control the height of the solution. At an industrial shape, this is done with a static knife and a rolling substrate. The plate is then submerged into an aqueous coagulation bath, causing the solvent and bath to mix. This drops the solubility of the polymer in the new solution, as it is dominated by the aqueous bath, causing it to fall out of solution. The permeation pattern then dictates the conformation of the final membrane, causing a largely asymmetric deposition with a dense surface and open substructure. By employing automated instruments with set delay between casting and submerging, as well as consistent curing time in the coagulation bath, industrial versions of this process improve the consistency of this process. For hollow fiber membranes, a slightly different manufacturing process has to be utilized. Namely, a spinneret shapes the fiber by shooting a jet of the coagulation bath, with a jet of polymer solution surrounding it. The inner jet forms the inner structure of hollow fiber through phase inversion rapidly as both streams continue falling to the larger coagulation bath, which precipitates the outer section of the fiber.

The three main components are the polymer, the solvent, and coagulation bath. The solvent and bath have to be miscible, and the polymer has to be soluble in the solvent but insoluble in the operating condition. For use with organic solvents, the space is still developing but early proposed polymers include poly(ether ether ketone) (Sun, et al. 2021), however, most uses of NIPS are in an aqueous environment as more complex manufacturing is more common in organic environments (Marchetti, et al. 2014). For aqueous environments, the polymer is often polyethersulfone (PES), polyvinylidene fluoride (PVDF), cellulose acetate (CA), polysulfone (PS), polyacrylonitrile (PAN), polyimide (PI), or polyether imide (PEI). Common solvents include dimethylformamide (DMF), n-methyl-2-pyrrolidone (NMP), dimethylacetamide (DMAc), dimethyl sulfoxide (DMSO), among others. The coagulation bath, by contrast, tends to mostly be just water, although alcohol can also be used (Drioli, Giorno and Macedonio 2019). These three components are the core of the NIPS process, but additives may also be present, especially in the polymer solution, colloquially called the dope, often has additives, which can vary from small molecules to another polymer like polyethylene glycol (PEG) or polyvinylpyrrolidone (PVP) (Ohya, Shiki and Kawakami 2009) (Lee, et al. 2015), to alter the final morphology of the membrane. The coagulation bath is usually water but can be any liquid in which the polymer is insoluble that is also miscible with the organic solvent, such as an isopropanol aqueous solution (Kars, Gühlstorf and Schwellenbach 2019). While the general effect of some variables is understood, the interplay between them has kept the understanding of the process largely empirical, though guided by the ternary phase diagram generated from a combination of cloud point experimentation and Flory-Huggins theory through transport models (Khansary, Marjani and Shirazian 2017) (Lee, Krantz and Hwang 2010) (Y. D. Kim, et al. 2001) (Karode and Kumar 2001) (McHugh and Miller 1995) (Cohen, Tanny and Prager 1979). This ternary phase diagram can give insights into the general category of final morphology, as an immediate demixing of the polymer results in more porous membranes while a delayed demixing results in denser, less porous membranes (Drioli, Giorno and Macedonio 2019). However, due to the rapid nature of phase inversion, it is difficult to

determine the exact composition of the solution in any given region, which makes model verification difficult. Accurate molecular simulation can be made to fill this gap, as it provides insight on the motion of system elements at a great resolution during extremely transient states.

2.2 Controlling Structure

Membrane structure matters greatly impacts performance and can be graded across a few metrics following from the basic equations of flow:

$$q = -\frac{k}{\mu}\nabla p \quad (1)$$

$$k = C * d^2 \quad (2)$$

Where q is flux, μ is the viscosity of the flued, Δp is the transmembrane pressure, C depends on path length, which is defined as size of the average path, and d is the pore size. Furthermore, selectivity is not a simple cutoff between larger particles that may not pass and smaller particles that can traverse freely, but rather a gradient, which can be tracked by percent breakthrough, which is not included in these fluid transport equations. This value is simply the percentage of particles that are removed from the feed during use and is largely driven by pore size and the length of the selective region of the pores. From this we can see the impact of pore characteristics. The largest pore is of course the least selective and having few large pores and many small pores reduces flux when compared to a membrane with a tighter pore distribution. As a high flux is highly desirable for industrial usage but must not sacrifice selectivity. Thus, C in equation (2) is the target, as a shorter path length will result in larger flux. While a thin membrane would significantly shorten the path length, extremely thin membranes are mechanically weak and would either break during initial handling or during operation at high pressure. Therefore, an ideal membrane must have a small pore distribution to maximize flux, the target pore size to improve selectivity, a thin selective layer, and a strong mechanical support. The support can be achieved using an asymmetric membrane, which can be produced one of several ways.

NIPS naturally forms an asymmetric membrane, which has a denser surface and more open substructure, the specifics of which are determined by dope composition, coagulation bath composition, and temperature (Drioli, Giorno and Macedonio 2019). Each system component has unique impact due to their interactions with the others. For example, if a solvent has a poor miscibility with the coagulation bath, this will result in delayed demixing when submerged, which tends to result in a porous structure with closed cells with a dense and thick surface. Conversely, a highly miscible solvent will result in rapid demixing, which tends to result in a highly porous structure with a more finely porous surface. These also tend to have many defects called macrovoids, which are structurally weak openings in the substructure (Drioli, Giorno and Macedonio 2019). The miscibility can be modelled using Hansen solubility parameters but are better modelled using free enthalpy of mixing (Mulder 2012), a process which we mirrored here. In short, while there are no hard definition, the rule of thumb is that a demixing resulting in the membrane turning opaque after more than 10-20s is delayed, while one that is faster than that is instantaneous (Drioli, Giorno and Macedonio 2019).

The solubility of a given composition of solvent/polymer/coagulation bath can matter greatly in determining the best material for desired properties. These can be mapped onto a triangular graph called a ternary phase diagram. A sample ternary phase diagram is provided in figure 2.1. In short, a ternary phase diagram has two main features: the binodal and spinodal curve. The binodal curve delineates the region where a homogeneous mixture can be achieved from the region where two phases exist: the solid polymer and liquid mixture. The spinodal curve, found within the two-phase region, delineates the metastable region which can resist basic thermodynamic stress. The binodal line can be determined experimentally by taking repeated cloud point measurements, which are taken by titrating water into a polymer/solvent solution until it turns cloudy, upon contact with the water droplet, the polymer falls out of solution. The polymer will then redissolve, or the solution will turn uniformly opaque. In the case of the former, another drop is

added. In the case of the latter, cloud point has been reached (Drioli, Giorno and Macedonio 2019). We can then compare the binodal lines to predict relative delays in mixing. For example, figure 2.2 shows the binodal lines of PVDF/water/solvent for a variety of solvents. From these, it can be determined that HMPA (Hexamethylphosphoramide) /PVDF will likely result in a denser membrane than the others as the stable region is much larger than any of the other tested solvents, resulting in delayed demixing (Drioli, Giorno and Macedonio 2019). Understanding this property is very important as rapid demixing has been linked to rapid demixing. However, that is not the only link. According to faster. However, we find the reverse experimentally, indicating other factors, such as kinetics, may play a factor (Drioli, Giorno and Macedonio 2019). Solvent is not the only liquid that can be changed in this system. The coagulation bath can be made from alcohol, which have a variety of effect. First, all alcohols have a higher molecular weight than water, slowing diffusion. This is particularly acute for larger alcohols. This leads to increasingly delayed mixing. Furthermore, small alcohols are stronger non-solvents than the larger ones, as the polar alcohol bond dominates the interaction more. This means that methanol can permeate better into the dope then cause a more drastic shift in solubility, resulting in higher void fraction (Drioli, Giorno and Macedonio 2019).

Setting aside the species of the components for now, increased polymer concentration affects the morphology by reducing the amount of open space in the membrane, a metric called porosity, as well as a less porous surface, increasing selectivity (Drioli, Giorno and Macedonio 2019). Adding a bit of nonsolvent to the dope prior to phase inversion also has an effect. This additive lowers the stability of the solution and brings it closer to the binodal line, which is going to make the demixing process much faster, effectively accelerating the formation process and resulting in more porous structures. While nonsolvent is not the common additive used for this in many cases, it illustrates the function of third compounds added to the dope in this manner (Drioli, Giorno and Macedonio 2019). The coagulation bath can be similarly targeted by adding solvent. This

conversely delays the formation process, as the composition of the membrane takes longer to reach the binodal line. This can result in otherwise porous membranes to become nonporous as more of the bath is replaced by the solvent. This has another interesting effect, however. The surface concentration of polymer decreases, resulting in more pores at the surface and less selectivity (Drioli, Giorno and Macedonio 2019). Temperature can also shift the membrane morphology. This effect, however, changes drastically from system to system due to its impact on two factors. Higher temperatures mean higher exchange rates, as per simple kinetics. This would suggest a shift to instantaneous mixing, which would result in a more porous membrane. However, higher temperatures also increase the stability of a given system, delaying demixing of the polymer out of solution. This would suggest a less porous membrane. As these two effects are in conflict and the degree to which one dominates the other changes from system to system and from temperature to temperature, this study must be done empirically (Drioli, Giorno and Macedonio 2019). Aside from that, none of the discussions presented above have taken into account the shifts in polymer conformation prior to the phase inversion thus far, which can also affect morphology.

Macrovoids are yet another concern for membrane manufacture. Macrovoids, as mentioned previously, are large porous structures that form in the more open substructure of polymer membranes, dominating the region and creating an obvious structural weakness that impacts the lifetime of the membrane. While not particularly bothersome in low pressure environments, the membrane risks failing at that point. Macrovoids form in a two-step process: initiation and propagation. While many factors play into initiation, it occurs beneath the surface during the initial liquid-liquid demixing process, likely as a polymer poor region which could have become a pore. From there, they grow downward through diffusion of solvent from the surrounding dope, while the back of the macrovoid solidifies. The front is thus semi stable while the back is solidifying, and the macrovoid stops growing if it encounters another stable nucleus or if the solidification

outpaces the liquid-liquid interphase. Due to the nature of this process, membranes that favor rapid demixing and more porous structures will also favor the formation of macrovoids. (Drioli, Giorno and Macedonio 2019). The composition of the system appears to be the single biggest determinant of macrovoid formation, but techniques exist to suppress it. Adding non solvent to the dope or solvent to the coagulation bath reduces their presence, as does the addition of specific additives. However, a large concern with macrovoid suppression is that while macrovoid are unwanted, so are the denser membranes that result from delayed mixing when manufacturing microfiltration or ultrafiltration membranes (Drioli, Giorno and Macedonio 2019).

2.3 Additives

Additives have seen much use in both the control of membrane structure and macrovoid suppression. Polyvinylpyrrolidone (PVP) and poly(ethylene glycol) (PEG) are commonly used for this purpose. While PVP has previously been linked with occasionally worsening macrovoid formation, it has significantly increased flux, and is believed to increase the demixing speed (Yeo, Lee and Han 2000). It has been suggested that PVP forms a thin wall between the pores that break upon drying, which further increases the pore size of the membranes (Wienk, et al. 1996). Despite behaviors suggesting a more rapid demixing from the more open pores, experiments have shown that when a blend of PES and PVP is treated as the polymer in a virtual ternary system, the binodal shifts radically to the right, a behavior that would suggest delayed demixing. This is done as PVP and PES have a very strong interaction with one another. If allowed to be more free, however, the gap returns to a more expected value for PES, which has led some to suggest and equilibrium value, which we see in cloud point experiments for blends (Wienk, et al. 1996). PVP was also found to improve fouling resistance to some degree, a property attributed to its hydrophilic nature when embedded in the membrane (Marchese, et al. 2003). However, follow up studies have shown that the contact angle for PVP-PES membrane is not significantly different from a pure PES membrane (Susanto and Ulbricht 2009). Contact angle is a standard way to

measure hydrophobicity and involves placing a water droplet over the surface, before measuring the angle of the droplet with the surface. A hydrophobic surface will of course result in a smaller footprint of water than a hydrophilic one, as the surface would repel the water, leading to the difference. It should be noted that Susanto and Ulbricht do not contradict the anti-fouling properties of PVP, but rather attribute it to some other property. PVP has other documented effects on membrane structure, as collated and tested by Susanto and Ulbricht (Susanto and Ulbricht 2009). PVP membranes have been found to shrink less when compared with the original thickness of the dope prior to the nips process then a purely PES membrane. The more open structure also collapsed more during high pressure usage, resulting in a higher flux decay than the baseline PES membrane or any of the other additives tested. However, the PES-PVP membrane was found to have a much higher normalized flux and saw better improvement after cleaning than its pure PES counterpart, although it was outperformed by the PES-PEG membrane. PVP also resulted in higher rejection for most size tested than PES, despite expectations to the contrary from its more open structure. A rougher surface is also observed with PVP membranes (Susanto and Ulbricht 2009) (Ochoa, et al. 2001).

2.4 Figures

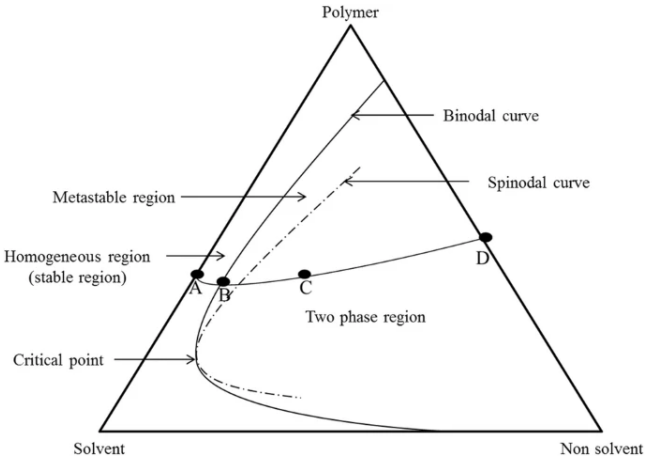

Figure 2.1 [credit (Nivedita, Ahamed and Joseph 2020)]:

The binodal curve separates the homogeneous single phase-region from the two-phase region. In the two phase region, the polymer is falling out of solution. The spinodal curve delimits the metastable region, where while not stable, resist thermodynamic fluctuations. The curve from point A to point D indicates the shift in composition of a given region as the solvent and coagulation bath mix. The boundaries in this phase diagram are dependent on the identity of all system components.

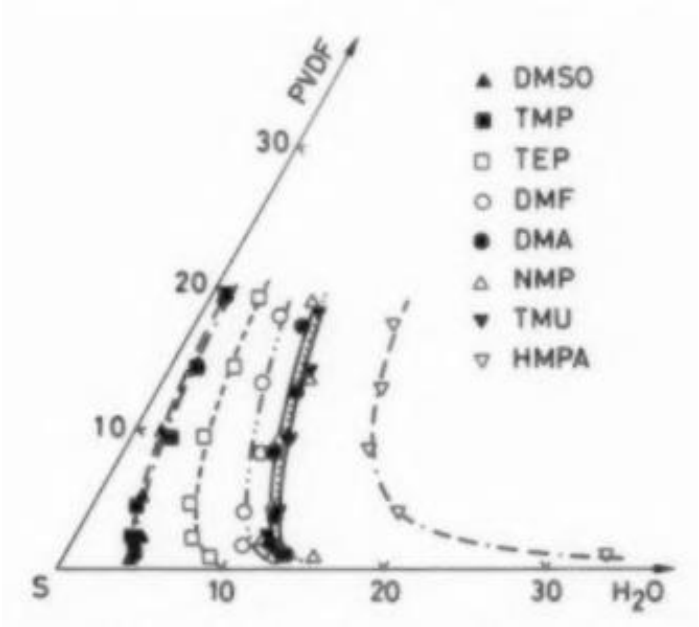

Figure 2.2 [credit (Bottino, et al. 1991)]:

The ternary phase diagram of PVDF, Water, and a variety of solvents, as determined experimentally by cloud point measurements by (Bottino, et al. 1991). Lines on the right of the image indicate a more stable mixture and likely delayed demixing, while those on the right are more likely to demix rapidly.

Chapter 3: Computational Approaches

3.1 Overview of Simulation Methods

Several simulation methods can be employed to gain insight into the formation process over a variety of time and length scales. Monte Carlo, which eschews mechanistic paths to determine the lowest energy state, has been used to obtain stable morphologies effectively by attempting different configurations at random and mapping out their energy level (Han, Wang and Zhang 2012). This allows for mapping out a free energy surface of a given system effectively but does not elucidate mechanisms well. Generating conformations purely at random would result in an oversampling of high energy states, however, as there are more high energy states than low energy states. To counteract this, a series of weighing mechanisms are employed. Monte Carlo is more of an umbrella term for a series of methods that use random inputs to map properties. The most common weighing algorithm utilized in molecular Monte Carlo calculations is the Metropolis algorithm, which accepts any change to a lower energy state, but generates a probability of accepting a higher energy state. Broadly speaking, that probability drops as the energy differential increases, preventing over sampling of high energy states (Wong and Liang 1997).

Molecular dynamic (MD) is another technique, simulating atomic motion very accurately based on standard molecular forcefields such as Chemistry at Harvard Macromolecular Mechanics (CHARMM), Amber, or individually calculated value from quantum calculations. These parameters track partial charges of molecules, as well as the equilibrium of the atomic bonds, angles, and dihedrals. While it has been used successfully to study systems very accurately, such as the balance of liquid-liquid and solid-liquid phase inversion of poly(vinylidene fluoride) (PVDF) (Sukitpaneenit and Chung 2009), the high level of fidelity incurs a high computational cost, but increasing computational power availability and the high degree of accuracy make this a very popular method. However, there are effective limits to both the physical space and time that can

be simulated within a reasonable time for any given computational resource. To circumvent this issue, coarse graining is required. Coarse graining refers to the practice of trading simulation detail for the sake of efficiency. While forms of coarse grained MD exist, we utilized dissipative particle dynamics (DPD), as it was explicitly written to allow for coarse-grained simulation for molecular systems which work at the meso-scale (Groot and Warren 1997). In this method, a group of atoms are taken as an aggregate, replacing all the forces of those individual atoms with a single repulsion value, as explained in detail below. This stands in contrast with even higher-level models which no longer account for molecular motion directly, such as phase field models. Phase field models estimate permeation speed to track changes in solubility instead (Cervellere, et al. 2019), which is a good way to estimate bulk behavior at even larger time scales. We have previously successfully utilized this method to generate a generic phase inversion system (Lin, et al. 2018), which then refined into a specific NMP/PES/water system (Tang, et al. 2020). For this work, we further expanded the size and time scale of that system to better observe such things as an increase in polymer molecular weight to a degree which our previous model could not achieve and is more akin to industrial uses. We also introduced an additive to the polymer solution, polyvinylpyrrolidone (PVP), a commonly used polymer additive. As it is more hydrophilic than PES and tends to result in larger pores, we expect to see some degree of shielding from the coagulation bath, resulting in that same behavior.

3.2 DPD Modeling

As described in our previous work (Tang, et al. 2020), DPD is a coarse-grained simulation technique for molecular simulation. In this method, a group of atoms are treated as single unit to allow for the simulation of a larger volume. They interact through soft conservative potentials, which are repulsions from one another dependent on Flory-Huggins solubility parameters. These are mediated through friction and stochastic (Brownian) forces. From there, the forces applied on

each unit are calculated, resulting in a net force vector for that time step, which then propagates to velocity and position following Newton's laws of motion through the following algorithm:

$$\vec{r_i}(t+\Delta t) = \vec{r_i}(t) + \Delta t\vec{v_i}(t) + \frac{1}{2}(\Delta t)^2\vec{f_i}(t) \quad (3)$$

$$\widetilde{\vec{v_i}}(t+\Delta t) = \vec{v_i}(t) + \lambda\Delta t\vec{f_i}(t) \quad (4)$$

$$\vec{f_i}(t+\Delta t) = \vec{f_i}\left(\vec{r}(t+\Delta t), \widetilde{\vec{v_i}}(t+\Delta t)\right) \quad (5)$$

$$\vec{v_i}(t+\Delta t) = \vec{v_i}(t) + \frac{1}{2}\Delta t\left(\vec{f_i}(t) + \vec{f_i}(t+\Delta t)\right) \quad (6)$$

In the above equations, $\vec{r_i}$ is the position of bead *i*, $\widetilde{\vec{v_i}}$ is the estimate of the velocity of bead *i*, $\vec{v_i}$ is the velocity of bead *i*, and $\vec{f_i}$ is the force vector acting on bead *i*. These can be interpreted as defining the new position in terms of the old one, as well as previous velocity and acceleration. Then the new velocity is estimated based on previous velocity and force. This is needed, as force calculations require a velocity value. The force is then calculated using that estimate, which is then used to get our final real velocity. To simplify the conversion from force to acceleration, these aggregates (beads) are defined to be of similar enough mass as to be treated as identical. Thus, we can define a custom mass unit which is equivalent to that mass, so that m = 1 in all cases, which allows us to remove that variable from all calculations. While this definition is not strictly true, it is true enough to be functional. As per our earlier work, we set the λ = 0.65 and the time step Δt = 0.01τ, which optimizes computational efficiency while maintaining temperature control. The value of λ was calculated in the original Warren and Groot paper which defined the DPD method and was empirically determined to improve system stability when compared to the base estimate of 0.5 (Groot and Warren 1997). τ is a reduced time unit based on the temperature and Boltzmann constant, and is equivalent to 7.9 ps. This principle is more thoroughly explained in our previous work (Tang, et al. 2020), but uses the following equation:

$$\tau = r_c\sqrt{\frac{M}{k_b T_{ref}}} \quad (7)$$

Where M is the molar mass of the particle as defined above, k_b is the Boltzmann constant, and T is 273 K, as per previous work. Three non-bonded forces act on the beads. These are applied pairwise in the direction of the other beads within a cutoff radius, r_c, and are the conservative, dissipative, and random forces. This value is based on the size of the beads. As defined in our previous work (Tang, et al. 2020) and the foundational Groot and warren paper (Groot and Warren 1997), the r_c is defined such as three beads fall in a single r_c^3 volume. This cutoff radius is also used as our basic length unit to simplify calculations and reduce computational resource usage and is equivalent to 0.84 nm. The conservative force is given by

$$\overrightarrow{F_{ij}^{C}} = \begin{cases} a_{ij}\left(1 - \frac{r_{ij}}{r_c}\right)\overrightarrow{e_{ij}}, & (r_{ij} < r_c) \\ 0, & (r_{ij} \geq r_c) \end{cases} \quad (8)$$

Which therefore simplified to

$$\overrightarrow{F_{ij}^{C}} = \begin{cases} a_{ij}(1 - \overrightarrow{r_{ij}}), & (r_{ij} < 1) \\ 0, & (r_{ij} \geq 0) \end{cases} \quad (9)$$

Where the distance vector $\overrightarrow{r_{ij}}$ is the distance between particle i and j, r_{ij} is the magnitude of said vector, and $\vec{e}_{ij}$ is the unit vector in the direction. The strength between particles i and j is introduced as a_{ij} and is characteristic of the identity of the two particles. This forms a linearly increasing repulsion within the r_c and approximates the repulsive region of a Lennard-Jones potential very roughly. The values for these are based on the Flory-Huggins parameter. χ_{ij} is the Flory-Huggins parameter between any two different bead type i and j. The types are each of the system components: P for PES (P)olymer, C for the water (C)oagulant, S for the NMP (S)olvent, and A is for the PVP (A)dditive. a_{ii} is the interaction between two particles of the same type, while the others are for mixtures. $a_{ij} = a_{ii} + 3.497\chi_{ij}$. These can be found in table 3.1, but in short, a lower χ would result in a weaker repulsion relative to other beads of the same type. A negative

value would even imply that the pair interaction is stronger than the interaction with other particles of the same type, promoting a strong association. The Flory-Huggins parameters are calculated according to the following equations, as per our previous work (Tang, et al. 2020). For solvent-solvent interactions, these are calculated based on the free energy of mixing, given here for generic solvents a and b (Altena and Smolders 1982) (Yilmaz and McHugh 1986).

$$\chi_{ab} = \frac{1}{x_a \varphi_b}\left(x_a \ln\left(\frac{x_a \gamma_a}{\varphi a}\right) + x_b \ln\left(\frac{x_b \gamma_b}{\varphi_b}\right)\right) \quad (10)$$

Where x is the mole fraction, γ is the activity coefficient, and φ is the volume fraction. As this can result in a range from 0.01 to 0.57 depending on the NMP/water make-up of any given region, these values were averaged to 0.27 for our system. This was a necessity, as we cannot recalculate the parameter mid simulation to account for shifting volume fractions. This is impractical as the simulation method does not allow for shifts on a software level and recalculating the value for every particle on every time step would be prohibitively expensive in terms of computing hours. For the polymer (pol) solvent (s) pair, the parameters are based on the following equation, which is based on the Hansen solubility parameter δ, as first described in 2002 (Lindvig, Michelsen and Kontogeorgis 2002)

$$\chi_{pol,s} = \frac{V_s\left[\left(\delta_{D,\ pol} - \delta_{D,\ s}\right)^2 + 0.25*\left(\delta_{P,\ pol} - \delta_{P,\ s}\right)^2 + 0.25*\left(\delta_{H,\ pol} - \delta_{H,\ s}\right)^2\right]}{RT} \quad (11)$$

Where the Hansen solubility parameter δ is divided into three components: δ_D, the dispersion component, δ_P, the polarity component, and δ_H, the hydrogen bonding component. The values for these for each of our components are listed in table 3.2. Different repulsion parameters create a differential preference for other components of the system, thereby modeling relative solubility. The other two forces active in DPD, the dissipative and random forces, are coupled to form a momentum conserving thermostat, as given by

$$\overrightarrow{F_{ij}^{D}} = -\gamma \omega^{D}(r_{ij})\left(\overrightarrow{e_{ij}} \cdot \overrightarrow{v_{ij}}\right)\overrightarrow{e_{ij}} \quad (12)$$

$$\overrightarrow{F_{ij}^{R}} = \sigma\omega^{R}(r_{ij})\theta_{ij}\overrightarrow{e_{ij}} \quad (13)$$

Where $\overrightarrow{v_{ij}} = \overrightarrow{v_i} + \overrightarrow{v_j}$, θ_{ij} is a random number with zero mean and unit variance, and γ and σ are coefficients for the dissipative and random forces respectively. σ is a coefficient for the random force and represents the noise in the system and is taken to 3.0 for temperature control, as in previous work. γ is a dissipative coefficient which is tied to σ as given by $\sigma^2 = 2\gamma k_B T$, while k_B is the Boltzmann constant and T is temperature. The two equations are also linked by their weight functions, $\omega^D(r_{ij})$ and $\omega^R(r_{ij})$, which follow the relationship $\omega^D(r_{ij}) = [\omega^R(r_{ij})]^2$, to satisfy the fluctuation-dissipation theorem. $\omega^R(r)$ can be functionally expressed as

$$\omega^R(r)\begin{cases}(1-r), & (r < r_c)\\ 0, & (r \geq r_c)\end{cases} \quad (14)$$

An additional force is added to polymer chains to represent the bonds. This is modelled as a spring force and represented by the following:

$$\overrightarrow{F_{ij}^{S}} = -K\overrightarrow{r_{ij}} \quad (15)$$

Where K is a spring constant, held to 2, as per previous work. There are no angle forces, however, as at this level of coarse graining, angles are free enough to not require modelling.

3.3 Tables

Table 3.1:

The Flory-Huggins (χ_{ij}) parameters for pair wise interaction and corresponding repulsion parameter (a_{ij}) between any two components I and j. P is PES, S is NMP, C is water, and A is PVP additive.

Temperature	χ_{PS}	χ_{PC}	χ_{PA}	X_{SC}	X_{SA}	X_{CA}
1.09	0.16	2.21	-1.02	0.27	0.35	0.48
a_{ii}	a_{PS}	a_{PC}	a_{PA}	a_{SC}	a_{SA}	a_{CA}
27.25	27.81	34.80	23.75	28.19	28.47	28.91

Table 3.2:

The molar volume and Hansen solubility parameter of each of our components (Hansen 2007), (Nasouri, Shoushtari and Mojtahedi 2015)

Species	$\delta_{D,\ dispersion}$ $(J/cm^3)^{0.5}$	$\delta_{P,\ polarity}$ $(J/cm^3)^{0.5}$	$\delta_{H,\ hydrogen}$ $(J/cm^3)^{0.5}$	Molar Volume (cm^3/mol)	δ $(J/cm^3)^{0.5}$
PES	19.6	10.8	9.2	15240	24.2
PVP	15.5	11.7	8.6	88.9	21.2
NMP	18	12.3	7.2	96.5	22.9
Water	15.5	6	42.4	18.0	47.9

Chapter 4: Simulation Investigation of Membrane Making

4.1 System Construction

The specific simulation system was composed of arrangements of the four components mentioned previously: water, NMP, PES, and PVP. These were arranged into two regions before the simulation: the coagulation bath and polymer solution. Both were periodic on two axes, the x and z axes, while non-periodic on the y axis. The coagulation bath was 90x90x90 r_c (75.6x75.6x75.6 nm), while the polymer solution consisted of 90x150x90 r_c (75.6x126x75.6 nm) These two boxes were generated through the molgen package, which generates the molecules in the desired density in a given volume. They were then allowed it homogenize over the course of 3 million time-steps (237 ns) independently from one another. Once homogenized, these two boxes are placed next to one another, with the interface replacing one of the non-periodic faces. The resulting box is 90x240x90 r_c (75.6x201.6x75.6 nm) as shown in figure 4.1. The simulation is then resumed, allowing the two boxes to mix, largely resulting in solvent homogenization as the polymer falls out of solution over the course of 3.6 million time-steps (284 ns) and becomes largely immobile.

As described in the definition of the DPD model given in the introduction section, a bead had to be created of roughly equal quantity for each component. This bead was normalized to the largest component, a PES monomer, and molecules of the other components were aggregated to roughly match in volume and ignore the mass inconsistencies. For NMP, this meant two molecules, for PVP, it was two monomers, and for water, it was ten water molecules. While this results in a molar volume of 200 $Å^3$, the mass of each bead was 232 Da for PES, 198 Da for NMP, 222 Da for the PVP, and 180 Da for the water. The interaction parameters for each component pair have been tabulated in table 4.1.

The resulting membranes were then analyzed using several techniques. First, there were the two-dimensional analyses, which were performed by taking small regions of 1 r_c (0.84 nm) in width and analyzing their contents, compiling the resulting values across the entire length of simulation area. These consisted of two dimensional pore sizes, which were calculated by determining the average distance between two PES regions separated by beads of another type for any given two dimensional slice. Similarly, a volume fraction was obtained by determining the proportions of the components in any given region. An average radius of gyration was calculated for each of the polymer types over time by utilizing the built in function of galamost, the simulation engine we used. This value is reflective of their affinity for the media in which they are located, as a smaller radius of gyration indicates a higher degree of repulsion away from the solution. The equation for radius of gyration is simply the average distance from center of mass for every bead in the polymer chain. Lastly, pore size distribution was determined by utilizing zeo++ (Willems, et al. 2012) (Pinheiro, et al. 2013), providing a histogram of the empty volumes within the membrane.

4.2 Experimental Sets

Molecular weight

The polymer solution was constructed with a consistent 12% PES and 88% NMP by volume. The coagulation bath consisted of pure water. The polymer chains varied in their molecular weight, with degree of polymerizations of 100, 150, and 200 monomers, which represents roughly 23, 35, and 46.5 kDa respectively (table 4.2). Our increase simulation volume allowed for longer chains to be studied when compared to our previous studies (Tang, et al. 2020), allowing for an interesting comparison to confirm our earlier findings.

Coagulant in the Polymer Solution

As mentioned above, a common tactic for suppressing macrovoid formation in the resulting membrane is to add some of the coagulant to the polymer solution in amounts below that which

would induce phase inversion (Kars, Gühlstorf and Schwellenbach 2019). To replicate this effect, polymer solutions containing 12% 46.5 kDa PES by volume were produced and phase inverted using a pure water coagulation bath. The remaining 88% was largely PES, but water was added, making up 0%, 1%, 5%, and 10% of the total volume, as described in table 4.3.

Solvent in the Coagulation Bath

Another common technique for controlling the formation process is to add solvent to the coagulation bath, decreasing the concentration gradient of the solvent across the interface with the coagulation bath. However, adding too much will cause the polymer to partially dissolve into the coagulation bath, decreasing the effective amount of polymer in the membrane. If the final concentration of does not reach past the binodal line, no phase inversion occurs. In an experimental system, the coagulation bath is orders of magnitude bigger than the polymer solution. However, due to size limitations, the bath is smaller than the polymer solution in the simulation, as seen in figure 4.1. Therefore, any amount of solvent added would greatly impact the formation process to a degree much greater than the same amount in an experimental coagulation bath. So, amounts added are much smaller than their experimental counterpart. The coagulation baths in table 4.4 phase inverted a 12% PES (46.5 kDa) and 88% NMP by volume solution. While 20% and 40% NMP were also attempted, the amount of NMP was too great to cause phase inversion.

PVP Additive

PVP, a commonly used polymer additive in the membrane fabrication process, was added to our model. The Flory-Huggins parameters were calculated using equation (11), as this is a novel component of the system not yet included in our published model (Tang, et al. 2020). For this experimental set, we contrasted two sets of data to measure the effects of replacing PES with PVP. The PVP and PES chains were ~33 kDa and ~46.5 kDa respectively, each representing

200 monomers. Due to the size difference of the monomers, PVP monomers were grouped into two monomers to one bead. Once homogenized, these solutions were phase inverted with a pure water coagulation bath. Their precise proportion by volume can be found in table 5a. Direct pore comparisons within these samples are impractical, however, as the added PVP skews the results because it is not counted as pore walls. This is because it would be washed out during use. Thus, table 5b is presented,

4.3 Results and discussion

Molecular Weight

The polymer chain length has caused some degree of concentration at the interface as seen in figure 4.2A, likely due to entanglement of the chains at the surface. It should be noted, however, that the 23 kDa chains and 35 kDa chains are far closer to one another than the 46.5 kDa, implying this effect is not linear. This is reflected in the two-dimensional pore size. For this measure, the most constricting part of the membrane is going define its restrictiveness and is noted as the largest takeaway. Although the two shorter polymers are not significantly dissimilar, the restrictive section of the 35 kDa system is much longer. The longest chain clearly shows the smallest pores, but the contrast is far less defined than that found in the volume fraction. While previous simulation studies also find a higher surface concentration (Tang, et al. 2020), this runs counter to experimental results that find larger pores that are more consistent throughout the membrane, making the structure less selective but more mechanically sound (Zhou, et al. 2010).

A clear decrease in 3D pore size is seen over time in figure 4.2C. This same motion is seen at an equivalent degree in all tested systems and will only be mentioned further if abnormal. At the last time step, 284 ns, we see in figure 4.2D that the three-dimensional pore size distribution for the whole membrane is fairly equivalent for all three membranes. As the subsurface is much larger than the interface, it dominates the distribution, which means that the subsurface structure is

equivalent for all three, which is again in contradiction with experimental results, which show an increase in pore size as the molecular weight increases (Zhou, et al. 2010). This effect is found to some degree in our previous study but is not statistically significant with this one (Tang, et al. 2020).

Figure 4.2E shows that the PES domain size for the three systems does not show statistically significant change. However, of note is the shape of the curve. Our previous study showed a rapid initial increase slowing down quickly (Tang, et al. 2020). However, we see three regions in this graph. A rapid increase in the average transitioning into a steady decline, before finally increasing once more at a linear rate. The most likely explanation is that, as an average, the domain size increases rapidly as large domain form when the water comes into contact with the polymer solution. Over time, this skin layer retreats away from the initial interface and the coagulant percolates through. This causes the sublayer to start coagulating in small clumps as well, creating many small domains. These bring down the average size, before merging with the large skin layer and each other, increasing the average once more. This effect would be minimal in a smaller simulation area due to the limited sub-layer volume. Our previous simulations, as described in previous publication, do not span the same time scale, which would explain the observation of the initial region alone. Our previous simulations also used a smaller size of box, which might contribute to this difference. Regardless of the cause, this pattern is observed on all simulated systems.

The average radius of gyration displayed in figure 4.2F shows an initial rapid decline due to the rapid drop in solubility, followed by a gradual decrease as water permeates further, as expected. It rapidly decreases initially as the polymer rapidly collapse on themselves on initial contact but are hindered by entanglement. The difference in initial position is attributable to the difference in chain length, as longer chains will naturally result in monomers being further from the center of mass.

***Water in the Polymer Solution**:*

The most predictable consequence of introducing water to the polymer solution prior to the simulation time is the collapsing of the average PES chain into a much more compact conformation prior to the main simulation time. This is in contrast with the rapid decrease in radius of gyration found in the solution without water when it first comes into contact with the coagulation bath, as seen in figure 4.3A. Furthermore, as the affinity of the solution for the polymer further decreases as more water is added, the conformation of the polymer become more compact. This suggest that the largest effect on initial conformation can be had with just a small amount of water but adding more will net some further collapse, as displayed in figure 4.3A. While further effects on radius of gyration were minimal, the domain size is altered significantly by the addition of water. Should the hypothesis for the domain development process proposed prior hold, the alterations found in figure 4.3B suggest that the smaller domains are starting to merge more quickly as you add more water. This makes physical sense, as the solution would have a much lower affinity much more quickly. Previous publications have cited adding water to the dope as bringing the solution closer to the binodal line, making the membrane develop faster (Drioli, Giorno and Macedonio 2019). This seems to hold for our results, as figure 5B shows the process occurring faster as more water is added.

When considering the last time step, we see two effects from adding water to the polymer solutions in evidence, as reflected in figure 4.3. First and foremost, a strong polarization of the domains into two polymer rich regions with a far more polymer lean central region, in contrast to the polymer rich interface followed by a less dense by still rich sublayer found in the low water systems and is strikingly obvious in figure 4.3C. Theory expects a more porous membrane as more water is added, a fact reflected in the 5% and 10% water having such a large gap (Drioli, Giorno and Macedonio 2019). This suggests a higher degree of cohesion amongst the polymer chains, reflected in the domain size average effect observed in figure 4.3D. The second effect is

a slight decrease in the thickness of the overall membrane. This is easily explained by the lower radius of gyration seen in figure 4.3A preventing entanglements down the line. These entanglements might slow down the rate of motion of the polymer fleeing the water, which would result in a thicker membrane for systems with less water. The two-dimensional pore size of these systems shown in figure 4.3D puts forward an interesting discrepancy. Namely, the 10% water solution, which has a the most concentrated PES region at the interface as shown in 6a, has larger pores than the 5% water solution, with 1.5 nm^2 and 1.3 nm^2 respectively. This implies that the 10% water solution subdivided its empty space into less pores than the 5% water solution and is in line with the increased amount in pores expected from theory (Drioli, Giorno and Macedonio 2019). The 5% water seems to be an outlier overall, being the only system to have smaller surface pores than the previous member in the series.

Solvent in the Coagulation Bath

As we increase the NMP concentration in the coagulation bath, the radius of gyration of these systems remains relatively unaffected, as seen in figure 4.4A. This indicates that while the affinity of polymer with the bath is increased, it is still insoluble in the final solution and collapses to a similar degree accordingly. The domain size (figure 4.4B), on the other hand, undergoes a major shift. Figure 4.3B shows a shorter time before the smaller subdomains merge, but 4.4B presents the opposite: a delay before the increase in average domain size is observed once more. This suggests that the increased affinity with the coagulation bath is lessening the pressure for smaller domains to merge. This result in line with expectations, as theory tells us that adding solvent to the coagulation bath slows membrane formation, causing a shift from instantaneous demixing to delayed demixing (Drioli, Giorno and Macedonio 2019). It is in examining the volume fraction that we see more striking structural change (figure 4.4C). Increased NMP in the coagulation bath resulted in the dense interfacial layer broadening significantly, both decreasing the surface concentration and making the membrane thicker. These changes are reflected in the two-

dimensional pore size (figure 4.4D) and would be expected of systems with more NMP in the water as theory suggests that the surface should be more porous (Amirabedi, Yegoni and Aghjeh 2013) (Drioli, Giorno and Macedonio 2019). However, this is where we also see a discrepancy with theory. The delay in demixing is meant to result in smaller pores in the subsurface (Drioli, Giorno and Macedonio 2019), an effect we do not see reflected in figure 4.4D. We instead observe equivalent pores in the substructure between all systems.

PVP Additive

While the radius of gyration is mostly equivalent for all purely PES systems (figure 4.5A) a small shift is observed in the initial radius and radius, showing that as concentration decreases, the slope becomes sharper. For example, the 10% PES system has a higher radius of gyration initially and lowers more dramatically over the course of the simulation. This is likely due to the crowding of higher systems. Interestingly, the PES radius of gyration is actually a little higher in systems with PVP than in ones with less PVP (figure 4.5C), although the pure PES system are lower. PVP has a larger radius of gyration at higher concentrations, likely due to its position deeper in the subsurface, which is a more hydrophobic environment. However, the systems with less PVP have a smaller radius of gyration, approaching that of PES, suggesting that the interfacial interactions between the bulk of the coagulation bath, PES, and PVP causes the PVP to bind strongly to the PES and mirror its conformation.

The domain size is larger for high polymer systems of pure PES (figure 4.6A), which makes intuitive sense as more polymer means they can more readily form large domains. However, the average comes down for all three until they reach the same point, at which point they start merging again. The reason for this phenomenon is unclear, however, as this suggests that an increasing amount of small domains are formed until a critical domain size is attained, which causes them to merge in a network. However, the size The PES domain size undergoes dramatic changes in the presence of PVP (figure 4.6B). It appears to affect two regions of the usual domain size progress:

the rapid initial formation of large domains and the decreasing average due to formation of small, scattered domains. The likely mechanism is the PVP, being more hydrophilic, surrounds the PES like a surfactant would a lipid in an aqueous environment. The increased amount of PVP relative to the PES allows for larger pores to form in the original interfacial layer lined with PVP. The PVP then helps the PES remain in solution longer, preventing the rapid formation of large amounts of smaller domains and allowing a gradual merging into larger ones.

Due to the variation in concentration of the polymers, volume fractions were normalized and now represent the percentage of the polymer of that type at the given location. Figure 4.7A-4.7C demonstrates a few behaviors. First, PVP is found to correlate to PES position. Second, this correlation is weaker at lower PVP concentrations (figure 9A), as the PVP will favor the interface with the coagulation bath. This suggests that PVP will remain at the interface until a saturation point is reached, at which point it will begin coating PES deeper in the substructure. Third, we also observe that as the PVP concentration increased, the size of the membrane does as well. This is in line with the observations made by Susanto and Ulbricht (Susanto and Ulbricht 2009).

4.4 Conclusion

Overall, our current results are in line with our previous publication in regard to the effect of the molecular weight on membrane formation. Furthermore, each of our experiments mirrored expected behavior from experimental systems. However, longer time scales and volumes revealed an interesting pattern in the PES domain formation. Three main regions were consistently observed across all our experiments that did not involve PVP. First, a rapid dramatic increase was found over the course of the first 50 ns, transitioning to a much slower decrease which continues over the course of around 120 ns. Finally, we see a linear increase during the remainder of the simulation time. Adding solvent to the coagulation bath and adding water to the polymer solution both altered the shape of these regions. Adding water to the polymer solution significantly shortened the period of decrease, while adding solvent to the coagulant delayed the

start of the linear increase at the end. PVP, however, seemed to alter the shape of the curve, suggesting that the behavior was specific to the trinary system.

The proposed explanation for the trinary behavior is that each region represents a different stage of the formation process. The rapid increase at the beginning is the initial contact at the interface causing a large domain to form quickly. The subsequent decrease, however, is due to the water infiltrating past the initial polymer barrier and into the sublayer, where it causes a series of small-scale phase inversions. Each burst quickly becomes diluted enough to prevent it from causing a large-scale phase inversion. A large quantity of domains are formed in this manner, causing the average size to decrease. Subsequently, the small domains begin merging with one another into larger ones. The third region begins when the rate of merging exceeds the rate of new domain formation.

The presence of water in the polymer solution prior to phase inversion would hasten this process, as the amount of water required to make larger domains becomes smaller. This behavior is observed in our experiment, as large domains quickly dominated, leaving two very dense regions and a polymer lean one between them. On the contrary, adding solvent to the coagulation bath prolonged the transition to the third phase, as it takes larger volume of the coagulation baths to cause phase inversion. We see this manifest in the volume fraction as well, where the PES was found to be more evenly distributed.

However, the domain formation process is fundamentally altered by the presence of PVP in the dope. We find adding any amount of PVP reduces the speed of the formation of the large domains in the initial phase inversion. This is likely due to the shielding of the more hydrophilic PVP stabilizing smaller PES domains, making them more viable in solution and slowing the merging process. Conversely, the secondary drop in domain size is hampered by PVP, even stopping entirely for the 10% PES 10%PVP solution. This is likely due to PVP creating more shielded

zones, which are more energetically favorable than a series of small domains. This makes for a proposed mechanism for the function of PVP in membrane formation.

4.5 Tables and Figures

Table 4.1:

The molar volume and Hansen solubility parameter of each of our components (Hansen 2007), (Nasouri, Shoushtari and Mojtahedi 2015)

Species	$\delta_{D,\ dispersion}$ $(J/cm^3)^{0.5}$	$\delta_{P,\ polarity}$ $(J/cm^3)^{0.5}$	$\delta_{H,\ hydrogen}$ $(J/cm^3)^{0.5}$	Molar Volume (cm^3/mol)	δ $(J/cm^3)^{0.5}$
PES	19.6	10.8	9.2	15240	24.2
PVP	15.5	11.7	8.6	88.9	21.2
NMP	18	12.3	7.2	96.5	22.9
Water	15.5	6	42.4	18.0	47.9

Table 4.2:

The PES chain length for the first experiment: chain length variation. All other variables are the same.

	Solution 1.1	Solution 1.2	Solution 1.3
Polymer chain size	~23 kDa (100 monomers)	~35 kDa (150 monomers)	~46.5 kDa (200 monomers)
Labeled as	23 kDa	35 kDa	46.5 kDa

Table 4.3:

The composition of the polymer solutions for the second experiment: adding water to the polymer solution. The coagulation bath remained pure water.

	Solution 2.1	Solution 2.2	Solution 2.3	Solution 2.4
PES	12%	12%	12%	12%
NMP	88%	87%	83%	78%
Water	0%	1%	5%	10%
Labeled as	0% water	1% water	5% water	10% water

Table 4.4:

The composition of the coagulation bath for the third experiment: adding NMP to the coagulation bath. The polymer solution remained 46.5 kDa PES at 12% and NMP at 88%.

	Solution 3.1	Solution 3.2	Solution 3.3
Water	100%	95%	90%
NMP	0%	5%	10%
Labeled as	0% NMP	5% NMP	10% NMP

Table 4.5a:

The composition of the polymer solution for set A of the fourth experiment: investigating the effect of PVP on membrane formation. Set A represents the experimental set and replaces NMP with PVP. The coagulation bath is pure water.

	Solution 4a.1	Solution 4a.2	Solution 4a.3
NMP	80%	80%	80%
PES	19%	15%	10%
PVP	1%	5%	10%
Labeled as	1% PVP	5% PVP	10% PVP

Table 4.5b:

The composition of the polymer solution for set B of the fourth experiment: investigating the effect of PVP. This set is the blank which has no PVP. The coagulation bath is pure water.

	Solution 4b.1	Solution 4b.2	Solution 4b.3
NMP	81%	85%	90%
PES	19%	15%	10%
PVP	0%	0%	0%
Labeled as	19% PES	15% PES	10% PES

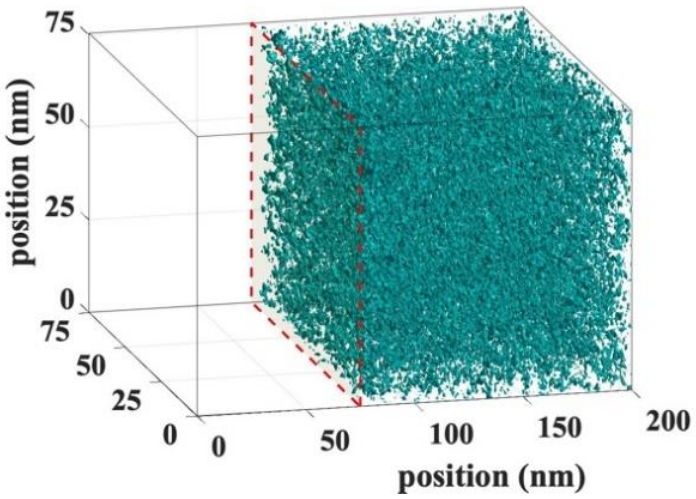

Figure 4.1:

A typical simulation system. 0 to 75 nm is the coagulation bath region, depicted as clear. The next region, the polymer solution, has PES and NMP is the section which includes color, depicting the polymer. The system in periodic on its long edges, but non periodic on its smaller ones.

Experimental Set 1

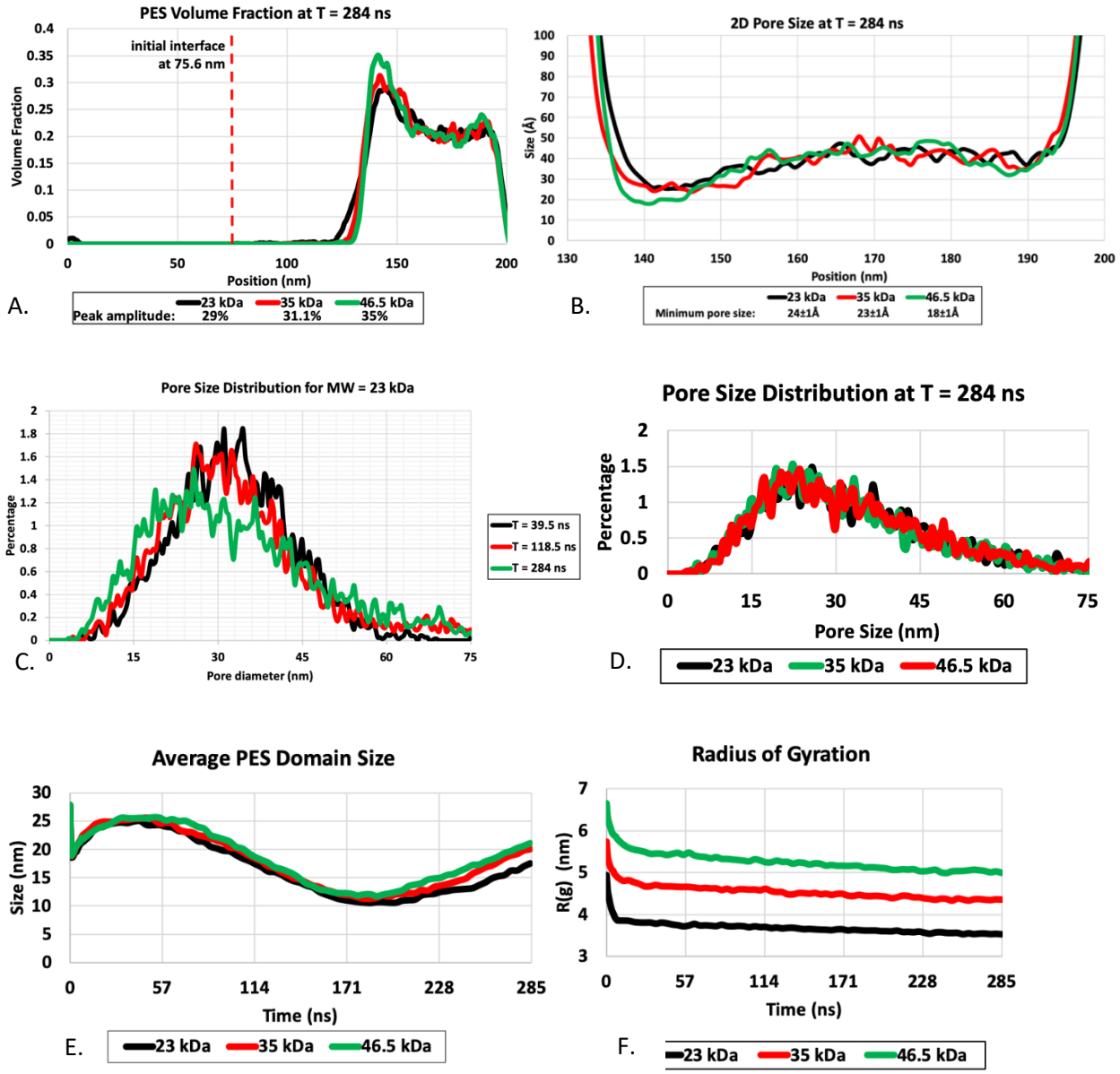

Figure 4.2:

A. The volume fraction of PES at the final time step, 284 ns, along with their peak amplitude for the first experiment.

B. The 2D pore size at the final timestep. This is calculated as the average distance between two regions of pure PES.

C. The 3D pore size over time for the 23 kDa system. This is measured as the radius of the largest sphere that can fit within the cavities of the structure. As phase inversion takes space, pores shrink. This pattern is repeated for every system.

D. 3D pore size for all 3 molecular weights at the last time step.

E. The average PES domain size over the course of the simulation progress. We see 3 main regions in this graph: an initial increase in domain size, stopping at around 50 ns, followed by a decrease which ends around 170 ns, and ending with an increase until the end of the simulation.

F. The radius of gyration shows a shift due to the difference in molecular weight but does not show any difference in slope or shape. The initial decrease is due to the contact with water causing an initial collapse, which then slows down as further minimizations occur.

Experimental Set 2

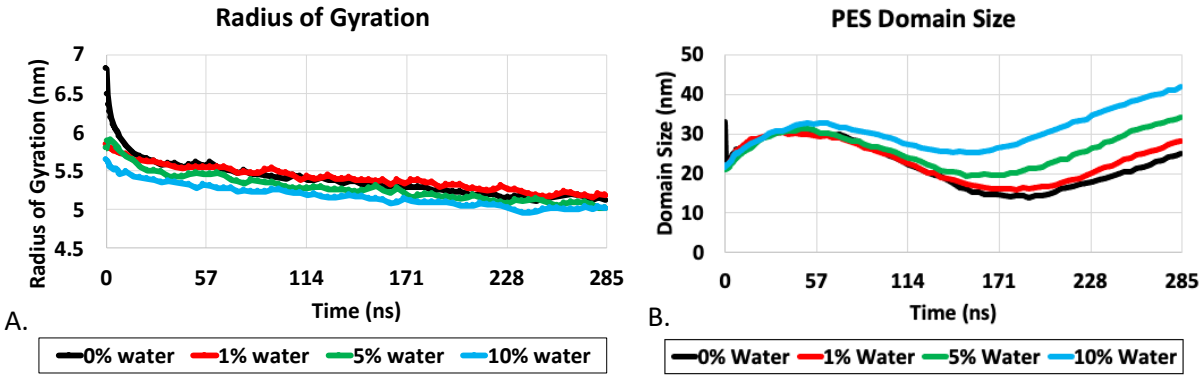

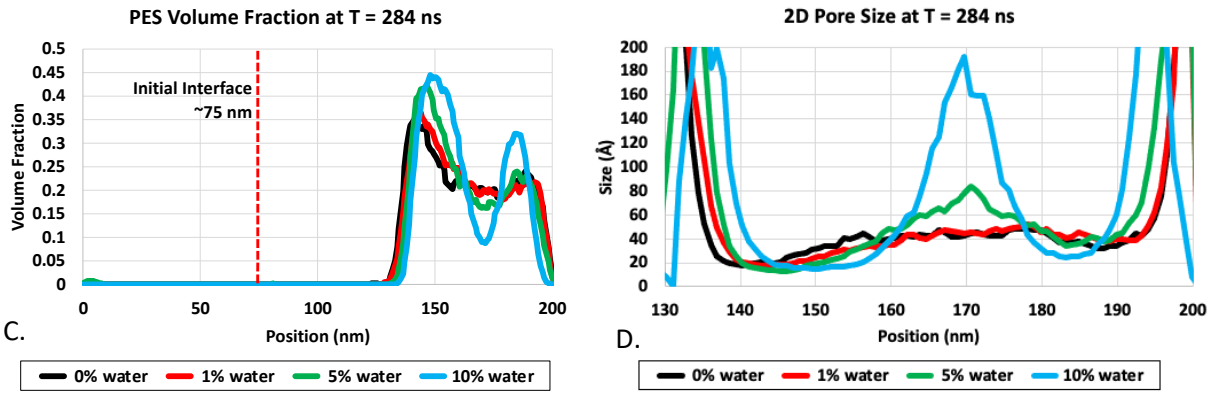

Figure 4.3:

A. The average radius of gyration of the PES chains over the course of the simulation. As expected, the lack of water resulted in a more relaxed initial state, which then normalized to a similar value as the system with 1% water in the polymer solution. We further observe additional water resulting in increasingly compact chains.

B. The average domain size for each of our systems show the same distinctive regions, but systems with more water in the polymer solution moved on the third region faster than systems with less water. This suggests that either fewer small domains form independently before merging or that they begin merging faster.

C. At the last time step, we see a high degree of polarization of the polymer in systems with a high water content. This is the physical representation of the larger domain sizes seen in figure 5b. This suggests a high degree of cohesion between the chains, a result that is consistent with the more hydrophilic environment.

D. The two dimensional pore size is largely agrees with the expected values based on the volume fraction, with a single exception. The 10% water system had a minimum point of 1.5 nm^2 while the 5% water system had a minimum of 1.3 nm^2. This suggests that the 10% had fewer but larger pores while the 5% system had more pores that were individually smaller.

Experimental Set 3

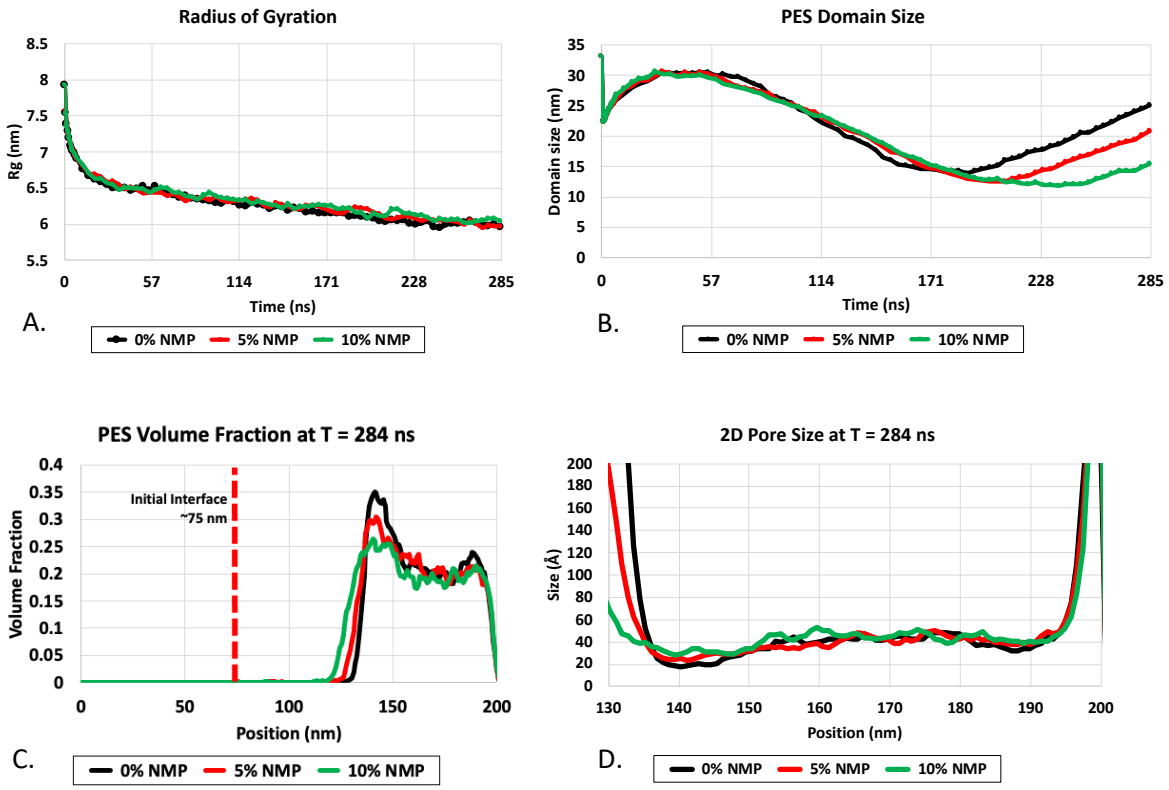

Figure 4.4:

A. The radius of gyration for these systems is almost equivalent. While a little higher with more NMP, it is still below the critical point for NMP/PES, so the radius can only increase so much

B. The average domain size takes longer to rise again as more NMP is added to the coagulation bath. This suggest that the more permissive solvent environment is allowing the smaller domains more time before the solubility drops enough to force merging with larger domains, slowing down the formation of the final superstructure.

C. The 2D PES volume fraction shows a very clear structural trend. As more NMP is added to the bath, the membrane becomes thicker and the interface becomes less pronounced

D. The wider polymer distribution found in 4C result in much wider pores, with the smallest pores being ~18 Å, ~23 Å, and ~29 Å for the 0%, 5%, and 10% NMP system respectively.

Experimental Set 4

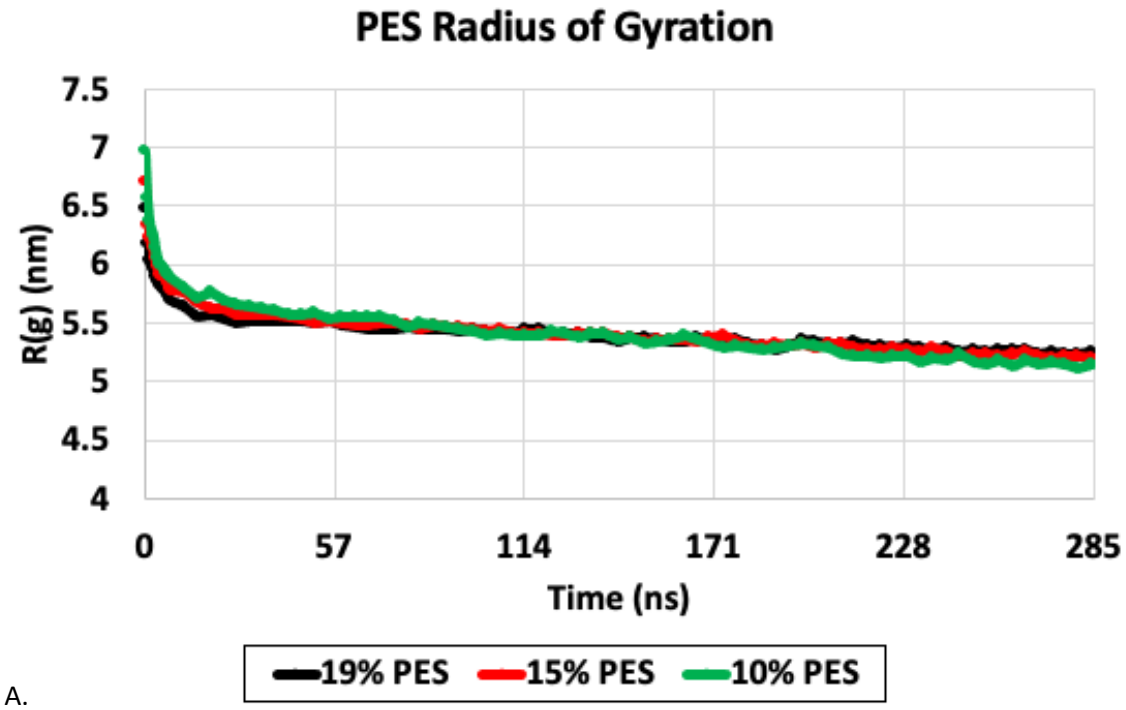

A.

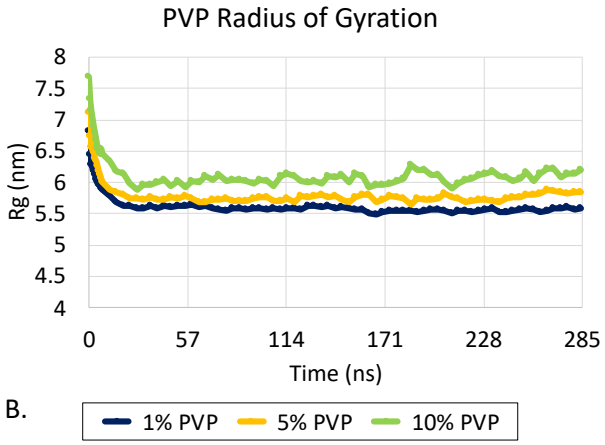

B.

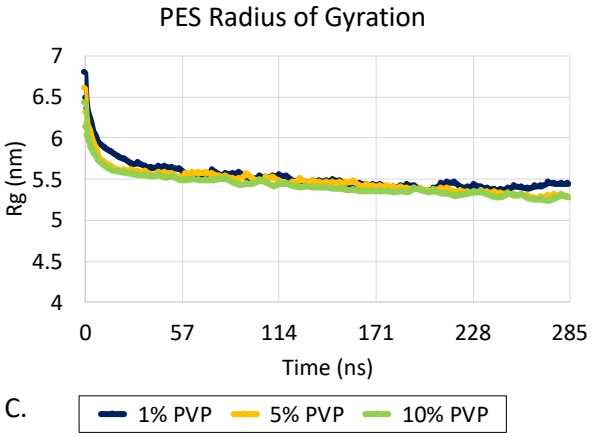

C.

Figure 4.5:

A. The PES radius of gyration in systems containing only PES. We see mild variation due to the concentration differences

B. The PVP radius of gyration in systems containing a total polymer content of 20%, with increasing amounts of PVP. We see a much lower radius of gyration at low concentration, likely due to PVP penetrating deeper into the polymer region, a more hydrophobic environment.

C. The PES radius of gyration in the systems described above. They remain at the same level as the lowest concentration of PVP.

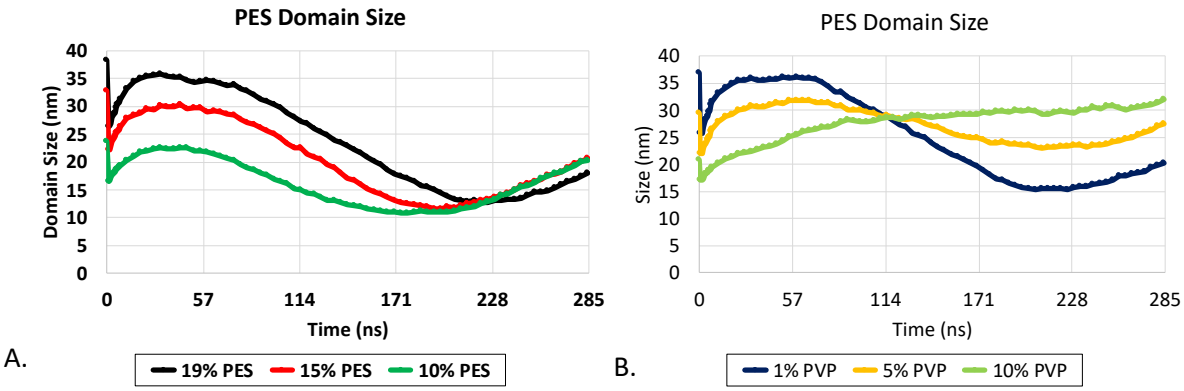

Figure 4.6:

A. The PES domain in the systems with no PVP. A larger initial domain is formed during contact with the coagulation bath, but all three roughly merge back at the end.

B. The PES domain size in the systems containing PVP. The overall shape of the curve is wildly altered. PVP lead to a slower initial coagulation as well as less smaller domains formed, likely due to its more hydrophilic nature shielding the PES.

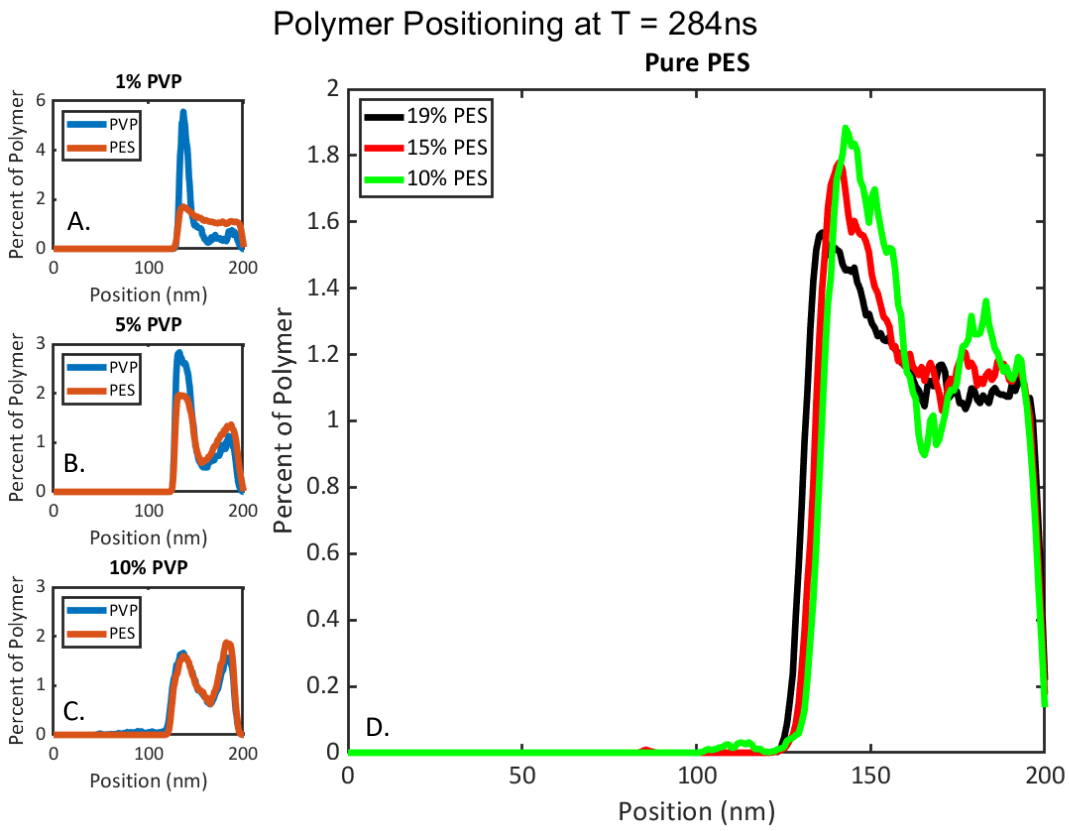

Figure 4.7:

A. The relative concentration of the polymers as a percentage of the total abundance. As each system had wildly varying concentrations of both PVP and PES, these values are normalized as a percentage. The PVP is generally found in regions containing PES, but is overabundant in the interface with the coagulation bath. For this system (1% PVP 19% PES pre-coagulation volume) this effect is particularly pronounced.

B. At the higher concentration of PVP (5% of total pre-coagulation volume) a similar behavior as in the 1% PVP system is observed, but the degree is not as pronounced. This suggests that the PVP favors the surface, but once a saturation point is reached, it will follow deeper into the sub structure.

C. Once the relative concentrations are equivalent, PVP fully permeates the PES and the positions match up one to one. However, a cavity begins forming at the core of the

membrane. This suggests a more open substructure that might have gone further but for the space limitations of the simulation.

D. In systems contain only PES, the descent from the concentration peak tends to be more gradual.

Literature Cited

Ahmad, Abdul Latif, Nuur Fahanis Che Lah, Suzylawati Ismail, and Ooi Boon Seng. 2012. "Membrane Antifouling Methods and Alternatives: Ultrasound Approach." *Separation and Purification Reviews* 318-346.

Alkhudhiri, Abdulah, Naif Darwish, and Nidal Hilal. 2012. "Membrane Distillation: A Comprehensive Review." *Desalination* 2-18.

Altena, F. W., and C. Smolders. 1982. "Calculation Of Liquid-Liquid Phase Separation In A Ternary System Of A Polymer In A Mixture Of A Solvent And A Nonsolvent." *Macomolecules* 1491-1497.

Amirabedi, Parya, Reza Yegoni, and Mir Karim Razavi Aghjeh. 2013. "Experimental Design Applied to Fabrication of PSf Membranes via NIPS Method ." *Journal of Textiles and Polymers* 24-30.

Ayyaru, Sicasankaran, and Young-Ho Ahn. 2017. "Application of Sulfonic Acid Group Functionalized Graphene Oxide to Improve Hydrophilicity, Permeability, and Antifouling of PVDF Nanocomposite Ultrafiltration Membranes." *Journal of Membrane Science* 210219.

Bottino, A., G. Camera-Roda, G. Capannelli, and S. Munari. 1991. "The formation of Microporous Polyvinylidene Difluoride Membranes by Phase Separation." *Journal of Membrane Science* 1-20.

Cervellere, M. Rosario, Yuan Hui Tang, Xianghong Qian, David M Ford, and Paul C Millett. 2019. "Mesoscopic simulations of thermally-induced phase separation in PVDF/DPC solutions." *Journal of Membrane Science* (Elsevier) 577: 266-273.

Cohen, Claude, G. B. Tanny, and Stephen Prager. 1979. "Diffusion-controlled formation of porous structures in ternary polymer systems." *Journal of Polymer Science: Polymer Physics Edition* 17 (3): 477-489.

Drioli, Enrico, Lidietta Giorno, and Francesca Macedonio. 2019. *Membrane Engineering.* Boston: De Gruyter.

Groot, Robert D, and Patrick B Warren. 1997. "Dissipative Particle Dynamics: Bridging the Gap Between Atomistic and Mesoscopic Simulation." *Journal of Chemical Physics* 4423.

Guillen, Gregory R., Yinjin Pan, Minghua Li, and Eric M. V. Hoek. 2011. "Preparation and Characterization of Membranes Formed by Nonsolvent Induced Phase Separation." *Industrial & Engineering Chemistry Research* 50: 3798-3817.

Guo, Wenshan, Huu-Hao Ngo, and Jianxin Li. 2012. "A Mini-Review on Membrane Fouling." *Bioresource Technology* 27-34.

Han, Yu, Jun Wang, and Hongdong Zhang. 2012. "Effects of kinetics coefficients on ternary phase separation during the wet spinning process." *Journal of Applied Polymer Science* 125 (5): 3630-3637.

Hansen, Charles M. 2007. *The Hansen Solubility Parameters (HSP) in Thermodynamic Models for Polymer Solutions.* Boca Raton: CRC Press.

Jiang, Bin, Binxing Hu, Na Yang, Luhong Zhang, Yongli Sun, and Xiaoming Xiao. 2021. "Study of Turbulence Promoters in Prolonging Membrane Life." *Membranes* 268.

Jiang, Xiaobin, Yushan Shao, Jin Li, Mengyuan Wu, Yuchao Niu, Xuehua Ruan, Xiaoming Yan, Xiangcun Li, and Gaohong He. 2020. "Bioinspired Hybrid Micro/Nanostructure Composited Membrane with Intensified Mass Transfer and Antifouling for High Saline Water Membrane Distillation." *ACS Nano* 17376-17386.

Karode, Sandeep K., and Ashwani Kumar. 2001. "Formation of polymeric membranes by immersion precipitation: an improved algorithm for mass transfer calculations." *Journal of Membrane Science* 187 (1-2): 287-296.

Kars, Catharina, Thorben Gühlstorf, and Jan Schwellenbach. 2019. "Influences of different preparation variables on polymeric membrane formation via nonsolvent induced phase separation." *Applied Polymer* 137 (28): 48852-48871.

Khansary, Milad Asgarpour, Azam Marjani, and Saeed Shirazian. 2017. "On the search of rigorous thermo-kinetic model for wet phase inversion technique." *Journal of Membrane Science* 538: 18-33.

Kim, Jeong F., Ji Hoon Kim, Young Moo Lee, and Enrico Drioli. 2012. "Thermally Induced Phase Separation and Electrospinning Methods for Emerging Membrane Applications: A Review." *AIChE Journal* 349-598.

Kim, Young Duk, Je Young Kim, Hwan Kwang Lee, and Sung Chul Kim. 2001. "A new modeling of asymmetric membrane formation in rapid mass transfer system." *Journal of Membrane Science* 190 (1): 69-77.

Lee, Eun Kyung, Vicki Chen, and A G Fane. 2008. "Natural Organic Matter (NOM) Fouling in Low Pressure Membrane Filtration — Effect of Membranes and Operation Modes." *Desalination* 257-270.

Lee, Hanyong, William Krantz, and Sun-Tak Hwang. 2010. "A model for wet-casting polymeric membranes incorporating nonequilibrium interfacial dynamics, vitrification and convection." *Journal of membrane Science* 354 (1-2): 74-85.

Lee, Jinwon, Bumjin Park, Jongpyo Kim, and Seung Bin Park. 2015. "Effect of PVP, lithium chloride, and glycerol additives on PVDF dual-layer hollow fiber membranes fabricated using simultaneous spinning of TIPS and NIPS." *Macromolecular Research* 23: 291-299.

Li, Yi, Shu He, Zhuang Zhou, Shaofeng Zhou, Shaobin Huang, Anthony G. Fane, Chunmiao Zheng, Yongqing Zhang, and Shuaifei Zhao. 2020. "Carboxylated Nanodiamond-Enhanced Photocatalytic Membranes with Improved Antifouling and Self-Cleaning Properties." *Industrial & Engineering Chemistry Research* 3538-3549.

Lin, Han-Han, Yuan-hui Tang, Hideto Matsuyama, and Xiao-lin Wang. 2018. "Dissipative particle dynamics simulation on the membrane formation of polymer–solvent system via nonsolvent induced phase separation." *Journal of Membrane Science* 548: 288-297.

Lin, Justin Chun-Te, Duu-Jong Lee, and Chihpin Huang. 2010. "Membrane Fouling Mitigation: Membrane Cleaning." *Separation Science and Technology* 858-872.

Lindvig, Thomas, Michael L Michelsen, and Georgios M Kontogeorgis. 2002. "A Flory–Huggins Model Based On The Hansen Solubility Parameters." *Fluid Phase Equilibria* 247-260.

Luo, Tao, Said Abdu, and Matthias Wessling. 2018. "Selectivity of Ion Exchange Membranes: A Review." *Journal of Membrane Science* 429-454.

Marchese, J., M. Ponce, N. A. Ochoa, P. Prádanos, L. Palacio, and H. Hernández. 2003. "Fouling Behaviour of Polyethersulfone UF Membranes Made with Different PVP." *journal of Membrane Science* 1-11.

Marchetti, Patrizia, Maria F. Jimenez Solomon, Gyorgy Szekely, and Andrew G Livingston. 2014. "Molecular Separation with Organic Solvent Nanofiltration: A Critical Review." *Chemical Reviews* 10735-10806.

McHugh, A. J., and D. C. Miller. 1995. "The dynamics of diffusion and gel growth during nonsolvent-induced phase inversion of polyethersulfone." *Journal of Membrane Science* 105: 121-136.

Mulder, Marcel. 2012. *Basic Principles of Membrane Technology.* Berlin, Germany: Springer Science & Business Media.

Nasouri, Komeil, Ahmad Mousavi Shoushtari, and Mohammad Reza Mohaddes Mojtahedi. 2015. "Thermodynamic Studies on Polyvinylpyrrolidone Solution Systems Used for Fabrication of Electrospun Nanostructures." *Advances in Polymer Technologies.*

Nivedita, S., Danish Ahamed, and Shiny Joseph. 2020. "Thermodynamic Analysis of Phase Diagram of H2O-DMF-PCL System: Investigation on the Influence of Inorganic Additives TiO2/MMT." *Journal of Materials Science* 5431-5444.

Ochoa, N. A., P. Prádanos, C. Palacio, J. Marchese, and A. Hernández. 2001. "Pore Size Distributions Based on AFM Imaging and Retention of Multidisperse Polymer Solutes:

Characterisation of Polyethersulfone UF Membranes with Dopes Containing Different PVP." *Journal of Membrane Science* 227-237.

Ohya, H, S. Shiki, and H Kawakami. 2009. "Fabrication study of polysulfone hollow-fiber microfiltration membranes: Optimal dope viscosity for nucleation and growth." *Journal of Membrane Science* 326 (2): 293-302.

Pinheiro, Marielle, Richard L. Martin, Chris H. Rycroft, Andrew Jones, Enrique Iglesia, and Maciej Haranczyk. 2013. "Characterization and comparison of pore landscapes in crystalline porous materials." (Journal of Molecular Graphics and Modeling) 44.

Rana, Dipak, and T Matsuura. 2010. "Surface Modifications for Antifouling Membranes." *Chemical Reviews* 2448-2471.

Shen, Zhisong, Binbing Han, and Ranil Wickramasinghe. 2004. "Cyanide Removal from Wastewater Using Gas membranes: Pilot-scale study." *Water Environment Research* 76: 12-22.

Sukitpaneenit, Panu, and Tai-Chung Chung. 2009. "Molecular elucidation of morphology and mechanical properties of PVDF hollow fiber membranes from aspects of phase inversion, crystallization and rheology." *Journal of Membrane Science* 340 (1-2): 192-205.

Sun, Yuxuan, Shengyang Zhou, Guorui Qin, Jing Guo, and Qifeng Zhang. 2021. "A Chemical-Induced Crystallization Strategy to Fabricate Poly(Ether Ether Ketone) Asymmetric Membranes for Organic Solvent Nanofiltration." *Journal of Polymer Science* 118899.

Susanto, Heru, and Mathias Ulbricht. 2009. "Characteristics, Performance and Stability of Polyethersulfone Ultrafiltration Membranes Prepared by Phase Separation Method Using Different Macromolecular Additives." *Journal of Membrane Science* 125-135.

Tang, Yuan-Hui, Eric Ledieu, M. Rosario Cervellere, Paul Millet, David Ford, and Xianghoung Qian. 2020. "Formation of polyethersulfone membranes via nonsolvent induced phase

separation process from dissipative particle dynamics simulations." *Journal of Membrane Science* 599: 117826.

Tirado, Miguel Levi Marré, Maria Bass, Maria Piatkovsky, Mathias Ulbricht, Moshe Herzberg, and Viatcheslav Freger. 2016. "Assessing Biofouling Resistance of a Polyamide Reverse Osmosis Membrane Surface-Modified with a Zwitterionic Polymer." *Journal of Membrane Science* 490-498.

Vatanpour, Vahid, Sayed Siavash Madeni, Rostam Moradian, Sirius Zinadini, and Bandar Astinchap. 2011. "Fabrication and Characterization of Novel Antifouling Nanofiltration Membrane Prepared from Oxidized Multiwalled Carbon Nanotube/Polyethersulfone Nanocomposite." *Journal of Membrane Science* 284-294.

Venault, Antoine, Yung Chang, Da-Ming Wang, and Denis Bouyer. 2013. "A Review on Polymeric Membranes and Hydrogels Prepared by Vapor-Induced Phase Separation Process." *Polymer Reviews* 568-626.

Wang, Yi, Xingya Li, Shuaifei Zhao, Zhendong Fang, Derrick Ng, Chaoxin Xie, Huanting Wang, and Zongli Xie. 2019. "Thin-Film Composite Membrane with Interlayer Decorated Metal–Organic Framework UiO-66 toward Enhanced Forward Osmosis Performance." *Industrial & Engineering Chemistry Research* 195-206.

Wang, Zhiwei, Jinxing Ma, Chuyang Y Tang, Katsuki Kimura, Qiaoying Wang, and Xiaomeng Han. 2014. "Membrane Cleaning in Membrane Bioreactors: A Review." *Journal of Membrane Science* 276-307.

Wienk, I. M., R. M. Boom, M. A. M. Beerlage, A. M. W. Bulte, C. A. Smolders, and H. Strathmann. 1996. "Recent Advances in the Formation of Phase Inversion Membranes Made from Amorphous or Semi-Crystalline Polymers." *Journal of Membrane Science* 361-371.

Willems, Thomas F., Chris H. Rycroft, Michaeel Kazi, Juan C. Meza, and Maciej Haranczyk. 2012. "Algorithms and tools for high-throughput geometry-based analysis of crystalline porous materials." (Microporous and Mesoporous Materials) 149 (1).

Wong, Wing Hung, and Faming Liang. 1997. "Dynamic Weighting in Monte Carlo and Optimization." *Applied Mathematics* 14220-14224.

Yeo, Ho-Taek, Sang-Taek Lee, and Myeong-Jin Han. 2000. "Role of a Polymer Additive in Casting Solution in Preparation of Phase Inversion Polysulfone Membranes." *Journal of Chemical Engineering* 180-184.

Yilmaz, L., and A. McHugh. 1986. "Analysis Of Nonsolvent–Solvent–Polymer Phase Diagrams And Their Relevance To Membrane Formation Modeling." *Journal of Applied Polymer Science* 997-1018.

Zhao, Shuaifei, Zhipeng Liao, Anthony Fane, Jiansheng Li, Chuyang Tang, Chunmiao Zheng, Jiuyang Lin, and Lingxue Kong. 2021. "Engineering Antifouling Reverse Osmosis Membranes: A Review." *Desalination* 114857.

Zhou, Chen, Zhengchi Hou, Xiaofeng Lu, Zhongying Liu, Xiaokai Bian, Liuqing Shi, and Liang Li. 2010. "Effect of Polyethersulfone Molecular Weight on Structure and Performance of Ultrafiltration Membranes." *Industrial & Engineering Chemistry Research* 9988-9997.

Zhu, Zhenya, Jialiang Jiang, Xudong Wang, Xiaonan Huo, Yawei Xu, Qingqing Li, and Lei Wang. 2017. "Improving the Hydrophilic and Antifouling Properties of Polyvinylidene Fluoride Membrane by Incorporation of Novel Nanohybrid GO@SiO2 Particles." *Chemical Engineering Journal* 266-276.